Journal of Fluids and Structures 17 (2003) 287–315

JOURNAL OF FLUIDS AND STRUCTURES

www.elsevier.nl/locate/jnlabr/yjfls

Booming and singing acoustic emissions from fluidized granular beds

A.J. Patitsas*

Department of Physics and Astronomy, Laurentian University, Sudbury, Ont., Canada P3E 2C6

Received 27 June 2001; received in revised form 9 July 2002

Abstract

The origin of the acoustic emissions from booming and singing sands is sought in the existence of modes of vibration in the granular beds composed of such sands. These granular beds are assumed to be sufficiently fluidized so that the equations of fluid mechanics are applicable. It follows from these equations and the concept of mechanical flux density that there are regions of failure in the granular beds where the fluctuation velocity is maximum. The regions of failure become the slip channels where the grain layers slip over each other towards regions of lower pressure, acting at the same time as energy sources of the acoustic emissions. The predicted frequency spectra of such emissions, which are defined primarily in the surface boundary layer, compare fairly well with those recorded experimentally. The acoustic phase velocity in the channels is close to 1 m/s, while that in the surface boundary layer is considerably lower. The origin of thermal moonquakes is sought in the squeezing of the granular beds in rock crevices. States of high compactness and high fluidity are predicted, the latter leading to the suggestion that crater erosion ridges on Mars are due to grain avalanches. The absence of boomability in snow avalanches could be due to the lack of a fluidized surface boundary layer. There is evidence to the effect that the boomability or singability of a granular bed is determined principally by the shape and surface texture of the grains, the rate of dissipation of the elastic modes of vibration in the grains and the degree of geometric confinement of the granular bed. The acoustic emissions occur during the latter phase of the slip or delatancy stage, which is preceded by the stick or compactness stage, when the elastic modes are excited.

1. Introduction

When wind-swept sand grains pile up on top of certain large dunes and then avalanche, a loud booming acoustic emission can occur with a dominant frequency in the range 50–200 Hz (Lewis, 1936; Bagnold, 1941; Humphries, 1966; Criswell et al., 1975; Lindsay et al., 1976; Haff, 1986; Nori et al., 1997; Sholtz et al., 1997 During van avalanche, blocks or slabs of sand, about 15 cm thick, break off and slide downhill. According to Lewis (1936), "the sound emission resembled the rumbling of a distant thunder from a few hundred yards away, while at closer distance it resembled that of an airplane or a motor lorry starting up". A more common acoustic emission of this nature occurs when the surface of certain beach sands is sheared with a plate, or even with the palm of the hand, at about 45° from the normal to the sand surface, or when it is stepped upon. Such sands are characterized as singing, sonorous, musical or squeaky, the dominant frequency being in the range 500–1500 Hz (Brown et al., 1961,1964; Nishiyama and Mori 1982; Miwa et al., 1983; plus all above citations).

The subject of the booming and singing sands was treated from the point of view of pure scientific curiosity until the lunar landings when seismic events, termed thermal moonquakes, were recorded near moon craters (Duennebier and

*Corresponding author. Tel.: +1-705-525-4098.
E-mail address: ansaari@cambrianc.on.ca (A.J. Patitsas).

0889-9746/03/$ - see front matter © 2002 Published by Elsevier Science Ltd.
PII: S0889-9746(02)00122-6

Nomenclature

B	bulk modulus of the fluidized granular bed
d	average grain diameter
e	coefficient of restitution
e_c	energy loss into heat during collision of two grains, Eq. (A.8)
E	Young's modulus
f	frequency of vibration
f_d	dominant frequency of vibration
h	depth of the fluidized bed
h_s	depth of the slip channel
I	energy converted into heat per unit volume per second due to grain-grain collisions, Eqs. (A.25) and (A.31)
I_{ij}	dimensionless parameters in the expressions for p and σ
p	total pressure in the granular bed
p_o	pressure in the granular bed due to external forces
p_a	pressure in the granular bed due to acoustic wave motion
q_1	dimensionless factor in the expression for σ, Eq. (A.17)
q_2	dimensionless factor in the expression for p, Eq. (A.18)
q_1'	equal to q_1 times $\bar{v}/\Delta u$
Q	mean fluidization energy flux density, Eq. (A.27)
r_c	collision rate of the grains $= 1/2(\bar{v}/s)$
R	average grain radius
s	average distance between grains
u_a	particle velocity due to acoustic wave motion
Δu	relative particle velocity between layers, in the flow direction
Δu_y	relative particle velocity between layers, normal to the flow direction, during delatancy
$\bar{v}$	random fluidization velocity
$\bar{v}_o$	amplitude of $\bar{v}$ in its variation with bed depth, Eq. (14)
$\bar{v}/\Delta u\|_o$	value of the velocity ratio $\bar{v}/\Delta u$ for which $\beta \to \infty$ for given μ and e, Eq. (12)
V	real acoustic phase velocity, Eqs. (16) and (20)
V_s	value of V at the center of the slip channel
V_c	complex phase velocity, Eqs. (4) and (24)
w	width of the slip channels
w_f	channel width factor, Eq. (18)
α	maximum surface displacement at the point of contact during collision of two spheres
β	extent of the fluidization, Eqs. (12) and (13), in the case of an unsingable granular bed. In the case of a singable-boomable bed, β is the distance between channels divided by 2π and approximately equal to the effective width of the slip channels, Eqs. (14), (18) and (19)
Γ	dimensionless parameter expressed in terms of μ and e, Eq. (A.31). It is a measure of the inelastic nature of the grain–grain collisions
Δ	dimensionless parameter measuring the mechanical energy leaving the granular bed during delatancy, Eq. (15)
η	coefficient of viscosity, Eq. (A.21)
θ_o	upper limit of the polar angle θ, Fig. A1 and Eq. (28)
λ_d	wavelength corresponding to the dominant mode of vibration, equal to the width of the channel, Eq. (18)
λ_B	Bagnold's linear concentration parameter $= d/s$
μ	coefficient of friction
ν	the Poisson ratio
ξ	particle displacement in wave motion
ρ	granular mass density
σ	shear stress, Eq. (A.16)
τ	relaxation time, Eq. (9)

ψ dynamic angle of sliding, Eq. (A.19)
ω angular frequency of vibration $= 2\pi f$

Glossary

Compactness and delatancy:
The coming together and the going apart of the grain-layers, during the state of flow in the granular bed, in an accordion-like motion perpendicular to the direction of flow.

Coefficient of restitution:
The ratio of the relative velocities of two spheres after and before a head-on collision.

Fluidization:
The state of a granular bed where the grains acquire a random velocity by becoming energized by flow velocity gradients, similarly to the thermal velocity of the molecules of a gas system.

Saultation or saltation:
The jumping, bouncing or leaping of the grains at the surface of a granular bed, which is energized by flow velocity gradients, or equivalently, by forcing the bottom of the bed to vibrate.

Stick–slip effect:
The effect where the resistive force of the granular bed on the penetrating plunger increases and decreases repetitively, resulting in a stick–slip motion of the plunger.

Sutton, 1974). These moonquakes begin rather abruptly about 2 earth days after the lunar sunrise and decrease rapidly after sunset. Their dominant frequency is about 5 Hz and their duration more than 60 s. However, the overall appearance of the time signals from these events resembles those from the booming and singing sands.

Sholtz et al. (1997), in a review paper, discussed at length the various hypotheses advanced to explain the physics of such acoustic emissions. Bolton (1889) argued that the acoustic emissions are due to vibrations of elastic air cushions between the grains. However, the emissions from a sand bed in a bell jar were shown to be independent of the air pressure in the jar (Criswell et al., 1975). Poynting and Thomson (1922) argued that in a closely packed array, composed of perfectly spherical and mono-sized grains, oscillations could arise when several, if not all, grain layers rise simultaneously to overtake those below and then fall back to the closely packed geometry. However, most of the acoustically active granular beds are not composed of such grains and those that are, beds of glass beads for example, are not necessarily acoustically active.

Bagnold (1966) advanced the only known semi-quantitative explanation of the mechanism responsible for such emissions. He assumed the existence of a single shear surface (slip plane or shear plane) at some depth h_s from the surface of the avalanching sand and reasoned that the collisions of the grains in the layer above the slip plane with those in the layer below result in a net upward force on the overburden above the slip plane. The momentum transfer in the upward direction from a given collision and the collision rate are proportional to the relative flow velocity Δu across the slip plane, resulting in a lift force on the overburden proportional to Δu^2. In effect, he argued that all grains on the upper layer collide nearly simultaneously with those on the layer below, as if they were nearly fixed in a rigid-like geometric configuration. Following a collective impact, the overburden rises a distance close to $d/14$ and then falls freely. The inverse of the time of free rise and fall is equal to the frequency of oscillation of the overburden, which varies as the square root of the gravitational constant g divided by the average grain diameter d. In the case of the forced singing sand, it was argued that the normal stress originating with the driving agent (the plunger) is much larger than the weight of the overburden, resulting in a much larger effective gravitational constant and thus a much larger emission frequency.

However, it is difficult to visualize how such a single slip plane can exist in a fluidized sand bed where the grain shape is far from spherical and the average grain diameter can vary from 0.1 to 0.6 mm (Brown et al., 1961,1964; Humphries, 1966; Ridgway and Scotton, 1973; Lindsay et al., 1976; Miwa et al., 1983; Leach and Chartrand 1994; Nori et al., 1997). The relatively recent report (Kilkenny et al., 1997) on the sonorous properties of silica gel powder, used for humidity control purposes, further exemplifies the point. Lewis (1936) claimed to have produced roaring sound from grains of common salt by heating sorted grains.

The single slip plane model cannot account for the complexity of the frequency spectra originating with the avalanching booming sand at the Sand Mountain in Nevada, USA, (Criswell et al., 1975), with the forced (impacted) sand in a dish (Qu et al., 1995), or with the frog sand recorded by this author. Further, such a simple model cannot account for the frequency of interruption in the acoustic emissions, which for the case of the frog sand is close to 10 Hz, the dominant frequency being close to 700 Hz. In the case of the avalanching booming sand, these frequencies are scaled down by a factor of about 10 (Lewis, 1936; Humphries, 1966; Criswell et al., 1975). The name "booming sand"

originated with the approximately 1 Hz frequency of interruption, otherwise known as "the beat frequency" (Sholtz et al., 1997). Evidently, a theoretical treatment of the subject ought to provide reasons why some sands sing with relative ease, while others sing with great difficulty and only under certain conditions of confinement.

Slip planes can be seen in the radiograph by Miwa et al. (1983) as channels of sand flow having finite width; this radiograph is included here in Fig. 3. It is estimated that the average width of these slip channels is about 5 mm and that there are close to 10 sand layers slipping over each other, assuming an average grain diameter $d = 0.5$ mm. It is stated in Miwa et al. (1983) that the sonorous emission coincides with the occurrence of such channels. If a channel is viewed as an elastic medium having width $w = 5$ mm and average acoustic phase velocity $V = 1$ m/s, the first overtone having wavelength $\lambda = w$ corresponds to the frequency of 200 Hz, which could be interpreted as the dominant frequency reported in Miwa et al. (1983).

When a granular bed is sheared by external forces, it becomes energized or fluidized in the sense that the grains acquire an average random velocity, $\bar{v}$, referred to as the fluctuation velocity or the pseudothermal velocity, not unlike the average thermal velocity in a molecular gas (Cowin, 1978; Ogawa, 1978; Savage, 1978; Shen and Ackermann 1982; Haff, 1983; Jaeger and Nagel 1992; Thompson and Grest 1992; Thompson, 1993). In this context, Haff (1983) utilized the equations of fluid mechanics in the study of mass flow in a fluidized granular medium. However, Jaeger and Nagel (1992) pointed out that, "such a procedure is fraught with difficulties and leads to instabilities in the equations". In a regular molecular gas, two molecules are assumed to collide only once in a given encounter. It will be seen below that in the case of the avalanching sand, about 50 collisions are effected between two grains during the time one grain overtakes the other. Evidently, in such a regime the Bagnold linear concentration parameter, $\lambda_B = d/s$, has to be considerably larger than 1, where s is the average grain separation distance. At the other end, λ_B has to be smaller than about 17 in order for flow to occur, according to Another major difference between the two systems is that in a molecular gas, the thermal velocity $\bar{v}$ is determined by the temperature T, while in a fluidized granular bed the pseudothermal velocity $\bar{v}$ is determined by the relative flow velocity Δu between adjacent layers. It will be seen that Δu lies in the neighborhood of 1 cm/s, implying stick–slip effects, according to Thompson and Grest (1992).

In deriving the equations for the pressure p and the shear stress σ from the equations governing the collision mechanics between elastic spheres (Goldsmith, 1960; Timoshenko and Goodier, 1970), the velocity ratio $\bar{v}/\Delta u$ emerges as a new independent variable. It will be seen that $\bar{v}/\Delta u$, the grain diameter d and the coefficients of dynamic friction μ and restitution e, completely characterize the granular bed.

Haff (1983) showed that when enough heat energy is generated in the grain mass due to high values of the shear stress σ, the fluctuation velocity $\bar{v}$ varies with the grain depth y in a periodic manner. It turns out that this periodic spatial variation provides the main key for unraveling the secrets of the booming and singing sand phenomena. Haff (1983) argued that a sound signal in the granular bed propagates with the velocity V, which is equal to the distance $d + s$ divided by the time interval, $s/\bar{v}$, required by a grain to travel the distance s, assuming that the velocity of sound inside the grains is relatively very large. He presented a plot of V versus y, which has a velocity well located at the center of the Couette flow geometry. Such a velocity well can be interpreted to correspond to a spring, or to an elastic bar, where the linear density ρ is constant but the spring constant k_s is smallest at the center and increases on either side.

The derivations of the expressions for p and σ in terms of $\bar{v}$, s and $\bar{v}/\Delta u$ are included in Appendix A in order to avoid cluttering Section 2 in the main text. For the same reason, the Navier–Stokes equation of motion, the energy equation and the derivation of the expression for the energy dissipation due to the inelastic nature of the grain–grain collisions are included in Appendix A. It is assumed that the lack of sphericity and at times the lack of near sphericity of the colliding grains affects only moderately the expressions for p and σ, implying that grain sphericity and size distribution can be set aside in the context of this study.

2. Theory

2.1. Wave motion

In order to investigate the existence of acoustic modes of vibration in a fluidized granular bed, it is necessary to determine the elastic properties of the medium, i.e., the bulk modulus B and the viscosity η as functions of the depth y (Figs 1 and 2). The volume density ρ was determined to be close to 1700.0 kg/m^3 in the case of the booming sand. The expression for the pressure p in a granular bed is

$$p = p_o + \rho g y + p_a, \tag{1}$$

where p_o is the externally applied pressure by the plate in Fig. 1 and p_a is the acoustic pressure. With $i = y$ in Eq. (A.22) and $u_y = u_a$ = the acoustic velocity, the following equation of motion is obtained, where there

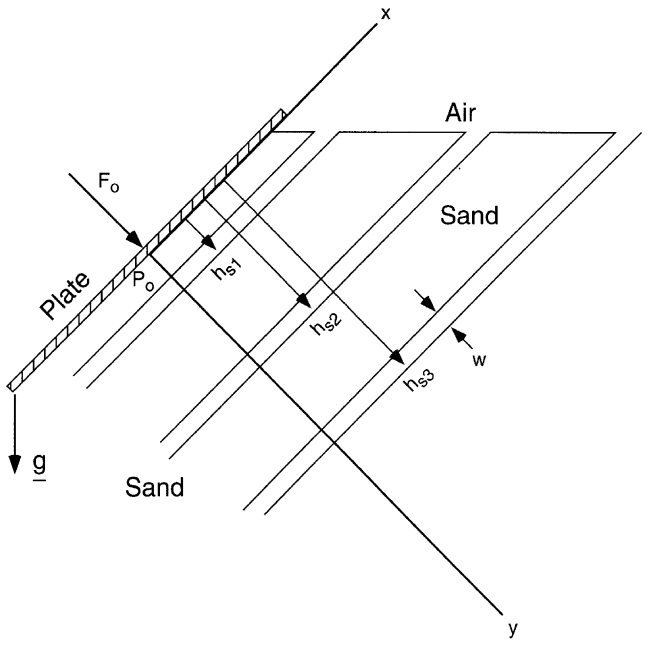

Fig. 1. Schematic of a rigid plate shearing the surface of a grain bed in a direction about 45° from the vertical. The pressure induced by the plate is p_o. The bands at the depths h_{s1}, h_{s2}, h_{s3} represent the slip channels in which the grains flow towards the surface of the sand bed. The width of the channels is shown as w.

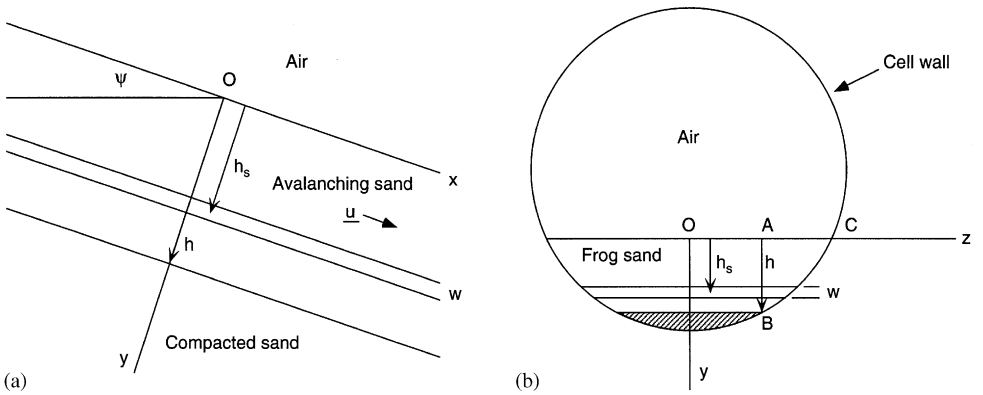

Fig. 2. (a) Schematic of a grain bed of depth h avalanching at the angle ψ from the horizontal direction. The overburden above the slip channel, at the depth h_s, is transported downhill by the slipping layers in the channel. The surface boundary layer is not shown. (b) Schematic of a vertical cross-section of the cylindrical cell containing the frog sand, held in a horizontal position. The inner diameter of the cell is about 5.9 cm, its length is 12 cm and the maximum depth of the sand-water mixture is about 1.5 cm. The shaded area represents the unfluidized section of the sand bed. The slip channel is at depth h_s.

is no variation with x, z

$$\rho \frac{\partial u_a}{\partial t} = -\frac{\partial p_a}{\partial y} + 2\frac{\partial}{\partial y}\left(\eta \frac{\partial u_a}{\partial y}\right). \tag{2}$$

The term $\rho u_k(\partial u_i/\partial x_k)$ was neglected compared to the term containing the coefficient of viscosity η, since the latter contains the differential $1/\partial y$ twice and $\partial y \approx d$. From Eq. (A.21), it follows that η is proportional to the collision rate

$\frac{1}{2}(\bar{v}/s)$, which is far from constant, as will be seen below. In order to get around this difficulty, the depth h in Fig. 2 is divided into small intervals Δy so that in one such interval η is fairly constant. Equation (2) then simplifies to

$$\rho\frac{\partial u_a}{\partial t} = -\frac{\partial p_a}{\partial y} + 2\eta\frac{\partial^2 u_a}{\partial y^2}. \tag{3}$$

From $u_a = \partial\xi/\partial t$, where $\xi(y,t)$ is the particle displacement, it follows that $\xi = -(\mathrm{j}/\omega)u_a$ where harmonic solutions, having the time dependence $\mathrm{e}^{\mathrm{j}\omega t}$, are assumed. From Kinsler et al. (1982), $p_a = -B(\partial\xi/\partial y)$, where B is the bulk modulus of the fluidized granular bed. From Eq. (3), the wave equation for ξ is

$$\frac{\partial^2\xi}{\partial t^2} = V_c^2\frac{\partial^2\xi}{\partial y^2}, \quad V_c = V\left(1+\mathrm{j}\frac{2\eta\omega}{B}\right)^{1/2}, \quad V = \left(\frac{B}{\rho}\right)^{1/2}, \tag{4}$$

where V_c and V are the complex and real phase velocities, respectively. It is shown in Kinsler et al. (1982) that the pressure p_a also satisfies the same wave equation. The general solution to the wave equation for p_a is

$$p_a = (C_1\mathrm{e}^{-\mathrm{j}ky} + C_2\mathrm{e}^{\mathrm{j}ky})\,\mathrm{e}^{\mathrm{j}\omega t}, \tag{5}$$

where the complex wavenumber $k = \omega/V_c$. With $\rho = m/(d+s)^3$, the equation of state (A.16c) becomes

$$p = q_2\frac{m}{(d+s)^2}\frac{\bar{v}^2}{s}. \tag{6}$$

Further, $B = \rho(\partial p/\partial\rho)$ and with $\partial p/\partial\rho = (\partial p/\partial s)(\partial s/\partial\rho)$

$$B = \frac{q_2}{3}\rho d^2\frac{\bar{v}^2}{s^2} \quad \text{or} \quad B = \frac{1}{3q_2}\frac{p^2}{\rho\bar{v}^2}, \tag{7}$$

where q_2 is given by Eq. (A.18). With $q_2 = 1$, $\rho = 1700\,\mathrm{kg/m^3}$, $d = 0.5\,\mathrm{mm}$, $\bar{v} = 10\,\mathrm{cm/s}$ and $\lambda_B = 10$, $B = 567\,\mathrm{N/m^2}$. If ξ assumes the simple expression $\xi = \xi_o\sin(ky')\mathrm{e}^{\mathrm{j}\omega t}$ about the point O' in Fig. 4, then the ratio of the amplitudes of the second and third terms in Eq. (3) becomes $B/(2\eta\omega)$. With $\eta = 2\,\mathrm{kg/(m\,s)}$ from Eq. (A.21), the third term can be neglected only for very low frequency emissions. The expression for the real velocity V in terms of p is

$$V = \sqrt{\frac{1}{3q_2}}\frac{p}{\rho\bar{v}}. \tag{8}$$

In Kinsler et al. (1982), the relaxation time τ is defined as $\tau = 2(\eta/B)$. It follows from Eqs. (A.16) and (A.21) that

$$\tau = 6\frac{q_1'}{q_2}\frac{s}{\bar{v}} \quad \text{or} \quad \tau = \sqrt{\frac{1}{3q_2}}\frac{6q_1'd}{V}. \tag{9}$$

It will be seen below that for the case of the frog sand, $d = 0.5\,\mathrm{mm}$, $V \approx 1\,\mathrm{m/s}$, $q_1 \approx 0.5$, $q_2 \approx 1.0$, $\bar{v}/\Delta u \approx 5$, resulting in $\tau \approx 4.3\times10^{-3}\,\mathrm{s}$ and $\omega\tau \approx 19$, with $f_d = 690\,\mathrm{Hz}$. The large value of $\omega\tau$ implies that Eqs. (3) and (7) may not be totally suitable to describe wave propagation in a fluidized granular bed.

It is evident from Eq. (8) that the random velocity $\bar{v}$ must be known as a function of y before any modes of vibration can be specified. After some algebra with two terms canceling out, the following differential equation for $\bar{v}$ can be obtained from Eqs. (A.29) and (A.30)

$$\frac{d}{q_2}p\frac{\mathrm{d}^2\bar{v}}{\mathrm{d}y^2} + \frac{d}{q_2}\frac{\mathrm{d}p}{\mathrm{d}y}\frac{\mathrm{d}\bar{v}}{\mathrm{d}y} + \frac{q_2}{q_1'}\frac{\sigma^2}{pd}\bar{v} - \Gamma\frac{p}{q_2 d}\bar{v} - 2p\frac{\partial u_y}{\partial y} = 0, \tag{10}$$

where σ, p, q_1', q_2, Γ are given by Eqs. (A.16)–(A.18) and (A.31) and $p = p_o + \rho g y$. The above equation is the same as Eq. (6.37) in Haff (1983) except for the terms involving μ, the term $\mathrm{d}\bar{v}/\mathrm{d}y$, resulting from $\mathrm{d}p/\mathrm{d}y \neq 0$ and the term involving u_y. Further, Eq. (10) is reducible to

$$\frac{\mathrm{d}^2\bar{v}}{\mathrm{d}y^2} + \frac{\rho g}{(p_o+\rho g y)}\frac{\mathrm{d}\bar{v}}{\mathrm{d}y} = -\frac{1}{\beta^2}\bar{v} + 2\frac{q_2}{d}\frac{\Delta u_y}{d}, \tag{11}$$

where

$$\frac{1}{\beta^2} = \frac{2}{d^2}\left[q_1\frac{\Delta u}{\bar{v}} - \Gamma\right], \tag{12}$$

and Δu_y is the difference in u_y between adjacent layers. It is assumed that Δu_y is nearly independent of y. It may be noted that u_y, in the context of the delatancy effect, is independent of the acoustic particle velocity u_a. It follows from

Eq. (A.8) that Γ is the measure of the inelastic nature of the grain–grain collisions. The parameter β can acquire a wide range of values, from ∞ when $q_1(\Delta u/\bar{v})$- $\Gamma \to 0$, down to d, when the same term approaches 1.

2.2. Forced sand

2.2.1. Unsingable forced sand $q_1(\Delta u/\bar{v}) - \Gamma < 0$

It is assumed that in this case there are no stick–slip effects, implying no compactness and delatancy effects, implying in turn that $\Delta u_y = 0$. Further, if $\rho g/2p_o \ll |1/\beta|$ and $\rho g/2p_o \ll 1$, then the solution to Eq. (11) is

$$\bar{v} = C_1 e^{-y/|\beta|} + C_2 e^{y/|\beta|}. \tag{13}$$

Since the fluidization energy is supplied by the plate at $y = 0$, in Fig. 1, it is reasonable to assume that $\bar{v}$ is maximum at $y = 0$, implying $C_2 = 0$. Clearly, β specifies the extent of the fluidization along y, and in this sense it can be labeled as the 'fluidization parameter'. Modes of vibration can exist in such a granular bed, but due to the high relaxation time they can only become excited by a driving force in resonance with them. From Eq. (8), the real velocity V increases exponentially with $y/|\beta|$. Effectively, the granular bed resembles a heavily damped spring whose spring constant increases exponentially with $[y/|\beta|]^2$.

2.2.2. Singable forced sand; $q_1(\Delta u/\bar{v}) - \Gamma > 0$

It can be concluded from the experimental study by Miwa et al. (1983) that, in this case, there are stick–slip and consequently compactness and delatancy effects in the granular bed, implying $\Delta u_y \neq 0$. The same assumptions, which result in Eq. (13), result in equations:

$$\bar{v} = \bar{v_o}\left(\cos\left(\frac{y}{\beta}\right) + \Delta\right), \tag{14a}$$

or

$$\bar{v} = \bar{v_o}\left(\sin\left(\frac{y}{\beta}\right) + \Delta\right), \tag{14b}$$

where

$$\Delta = 2q_2\left(\frac{\beta}{d}\right)^2 \frac{\Delta u_y}{\bar{v_o}}. \tag{15}$$

Clearly, Δ has to be larger than 1 for $\bar{v}$ to remain positive for all y/β. With $\Delta = 1$, $q_2 = 1$, $\beta/d = 10$, it follows that $\Delta u_y/\bar{v_o} = 1/200$. This justifies the assumptions that $u_y \ll 1$ and $u_y \ll u_x$ in Eq. (A.26). The fluctuation velocity $\bar{v}$ has not been expressed as the superposition of the two solutions presented above, since in a highly viscous fluidized bed $\bar{v}$ is nearly 0 at the floor of the bed. Which one of the two solutions applies depends on the value of β, as will be argued below. In either case, the fluidization parameter β can be interpreted as the wavelength of the spatial variation of $\bar{v}$ with y/β divided by 2π. It is also the distance between channels divided by 2π and approximately equal to channel width, as shown below.

It can be verified that the pseudoheat flux density Q, Eq. (A.27), points towards $-\hat{y}$ or $\hat{y}$ at $y = 0$, if Eq. (14a) or (14b) is adopted, respectively. If β is sufficiently large so that the first slip channel lies below the floor of the granular bed, or if it is sufficiently small so that the slip channels are crowded near the surface, then Eq. (14a) would apply. Effectively, without the presence of a slip channel in the granular bed there is no means for the dissipation of the energy flux into the sand mass, resulting in a highly energized boundary layer. Fig. 1(b) in Jaeger and Nagel (1992) and Fig. 3(b) in this report appear to be good representations of such a case. In the report by Jaeger and Nagel, mustard seeds are induced to avalanche down an inclined plane, with only three layers on the surface participating in the avalanche. When Eq. (14b) is applicable, the regions of high velocity $\bar{v}$, i.e., the regions of the slip channels, otherwise known as the regions of weakness or failure, are at $y/\beta = \pi/2$, $5\pi/2$ etc. It can be verified that the energy flux Q, Eq. (A.28), points towards these regions from either side, resulting in large energy concentration in these relatively narrow bands.

The first slip channel at $h_{s1} = (\pi/2)\beta$, in Fig. 1, would not be realized since it is too close to the plate where it would overlap with the boundary layer or with turbulent grain flow, as illustrated in Fig. 3(a). The second and third channels occur at $h_{s2} = (5\pi/2)\beta$ and at $h_{s3} = (9\pi/2)\beta$, respectively. When the pressure p_o is sufficiently large, the sand mass in the regions of weakness begins to flow towards the sand surface where the pressure is lower and thus the slip channels are realized, as illustrated in Fig. 3(a).

It follows from Eqs. (8) and (14b) that

$$V = V_a F_a, \tag{16}$$

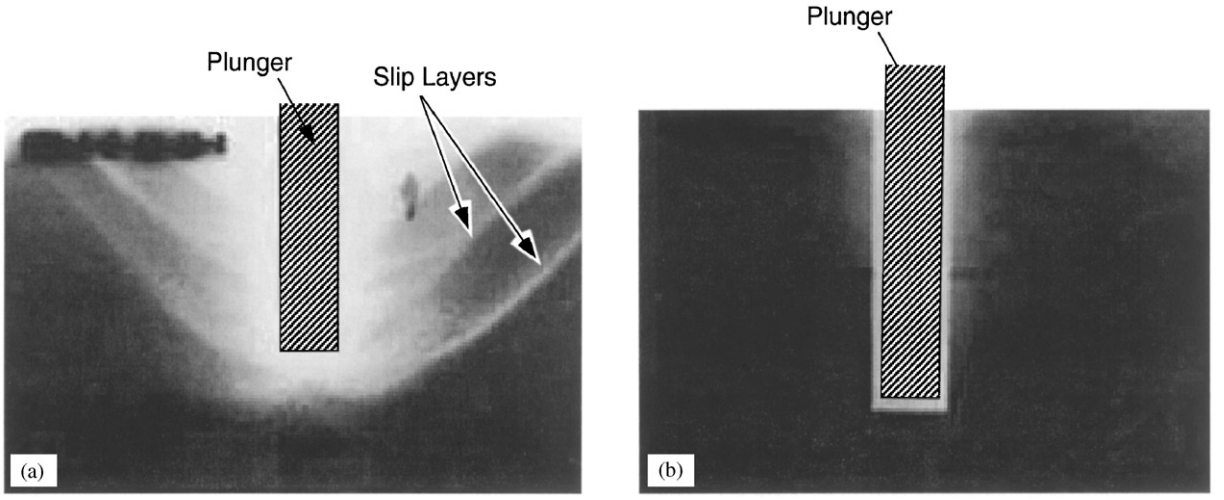

Fig. 3. X-ray radiographs depicting a rectangular plunger, 3 cm wide by 5 cm deep, impacting on a bed of sonorous and silent sands. The average width of the slip channels is estimated to be 4.8 mm. The slip channels are shown as slip layers in the report by Miwa et al. (1983). Reproduced by permission of the principal author. (a) Musical sand. (The number of distinct, and periodical occurence, of slip layers corresponds to the frequency of the sound.) (b) Silent sand has no slip layers.

where

$$V_a = \sqrt{\frac{1}{3q_2}}\frac{p_o}{\rho \bar{v}_o}, \qquad F_a = \frac{1}{(\sin(y/\beta) + \Delta)}. \tag{17}$$

In the slip channel, V is written as

$$V_s = \lambda_d f_d = w f_d, \quad w = w_f 2\beta, \tag{18}$$

where λ_d is the wavelength of the dominant mode for which the pressure p_a peaks at the center of the slip channel. It can be estimated from Fig. 4 that the effective width w of the channel is about 2β. However, the shape of the velocity well and the large relaxation time result in a correction factor w_f close to 0.5, as will be established below.

2.3. Avalanching sand

2.3.1. Unboomable avalanching sand; $q_1(\Delta u/\bar{v}) - \Gamma < 0$

In the cases of Fig. 2, p_o assumes the value 0 in Eq. (11). When Eq. (11) is multiplied by y^2 and the substitution $z = y/\beta$ is effected, the resulting equation is the modified Bessel differential equation of zero order having the solutions $I_o(y/\beta)$ and $K_o(y/\beta)$. The modified Bessel function of the first kind $I_o(y/\beta)$ assumes the value 1 at $y/\beta = 0$ and rises very sharply with increasing y/β (Abramowitz and Stegun, 1964). More conventional expressions for $\bar{v}$ and V can be obtained from the second solution $K_o(y/\beta)$. The difficulty with $K_o(y/\beta)$ becoming ∞ at $y/\beta = 0$ can be bypassed by assuming the existence of a surface boundary layer, so that the limit $y/\beta \to 0$ need not be considered.

2.3.2. Boomable avalanching sand ; $q_1(\Delta u/\bar{v}) - \Gamma > 0$

The solutions in this case are

$$\bar{v} = \bar{v_o}\left[J_o\left(\frac{y}{\beta}\right) + \Delta\right] \tag{19a}$$

or

$$\bar{v} = \bar{v_o}\left[Y_o\left(\frac{y}{\beta}\right) + \Delta\right], \tag{19b}$$

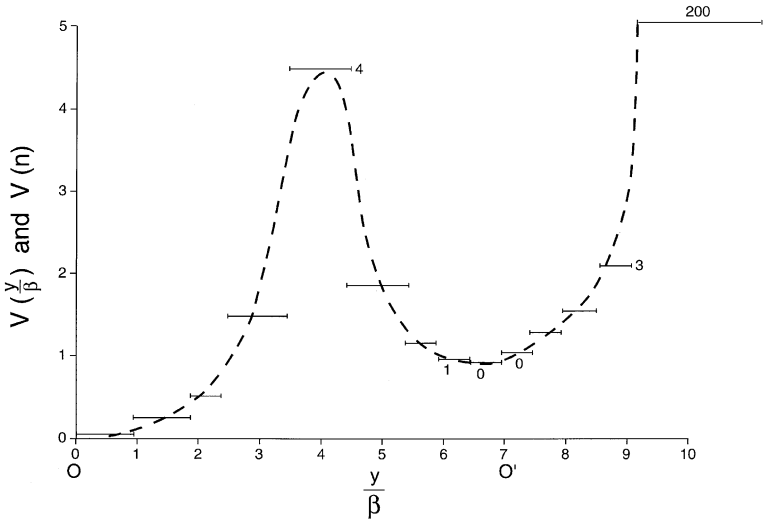

Fig. 4. The broken line represents the function V, Eq. (20), which is a measure of the complex phase velocity V_c, Eq. (24), describing an avalanching granular bed. The depth of the channel h_s corresponds to the point O'. The horizontal bars depict the intervals in which the linearized wave Eq. (4) can be assumed to hold. V_n is the phase velocity at the center of the nth interval. To the left of O, $V = 333$ m/s, i.e., the phase velocity in air at standard conditions.

where $J_o(y/\beta)$, $Y_o(y/\beta)$ are the ordinary Bessel functions of zero order. The second solution is not applicable since $Y_o(y/\beta) \to -\infty$ as $y/\beta \to 0$. From Eqs. (8) and (19a) it follows that

$$V = V_b F_b\left(\frac{y}{\beta}\right), \tag{20}$$

where

$$V_b = \sqrt{\frac{1}{3q_2}}\frac{g\beta}{\bar{v}_o}, \quad F_b = \frac{y/\beta}{J_o(y/\beta) + \Delta}. \tag{21}$$

Except for a constant factor, V varies with y/β as shown in Fig. 4 by the broken line. The center of the first velocity well lies just under $y/\beta = 7.0$ and the centre of the second just under $y/\beta = 13.3$, where the second maximum of $J_o(y/\beta)$ occurs, etc. It follows from the equation $p_a = -B(\partial\xi/\partial y)$ that p_a, $\partial\xi/\partial y$ and $\partial u_a/\partial y$, corresponding to the first overtone, all peak at the center of the channel at O'. Therefore, the first overtone plays an important role in the capacity of the layers to slip over each other, facilitating at the same time the energy transfer from gravitational potential energy to vibrational energy. Effectively, a self-generating resonance process takes place, which can explain the enormous vibrational energy developed during prolonged slides, despite the high viscosity characterizing the sand bed. In the neighborhood of the centre of the slip channel, $V = V_s$ where

$$V_s = \sqrt{\frac{1}{3q_2}}\frac{7}{0.3 + \Delta}\frac{g\beta}{\bar{v}_o}, \tag{22}$$

where 0.3 is the value of $J_o(y/\beta)$ at its first maximum. V_s can also be expressed as in Eq. (18). It has been remarked that wave Eq. (4) holds only in a small interval $\Delta y/\beta$, where the viscosity η and the bulk modulus B are approximately constant. In Fig. 4, such intervals are shown by horizontal bars where the smaller intervals have length 0.5 and the larger ones are twice as long. For better computational stability, the origin was chosen at O'. The intervals are enumerated from 0 to 8 going left from O' and from 0 to 3 going right. The velocity to the left of the third interval was chosen to be 200 m/s to correspond to the phase velocity in unfluidized sand beds (Winterkorn and Fang 1975). Its exact value is not critical as long as it is much greater than $V(0)$ at the centre. From Eq. (20), the function V at the center of the nth interval is

$$V(n) = \frac{0.3 + \Delta}{7} V_s \frac{y(n)/\beta}{J_o(y(n)/\beta) + \Delta}. \tag{23}$$

From Eqs. (4) and (9), the corresponding complex phase velocity is

$$V_c(n) = V(n)\left[1 \pm \mathrm{j}6q_1'\left(\frac{1}{3q_2}\right)^{1/2}\frac{\omega d}{V(n)}\right]^{1/2}, \tag{24}$$

where the sign of j has to be adjusted so that there is attenuation, not enhancement, along the wave propagation. In order to determine the natural frequencies of vibration f_i, the standard procedure (Kinsler et al., 1982) was followed in equating the pressure p_a and the particle velocity u_a at the end of a given interval to those at the adjacent end of the adjacent interval. The procedure leads to a system of linear equations, where the coefficients can be determined for given values of $\beta, \Delta, V_s, q_1', q_2, \rho, d$ and $\omega = 2\pi f$. The frequencies f_i were determined by varying f until the determinant of the coefficients acquired a minimum value. In the determination of $p_a(y/\beta)$ from the same equations, the pressure coefficient in air to the left of O, in Fig. 4, was assigned the value 1.

3. Results

3.1. Unforced sands

3.1.1. Frog sand

The shaded area in Fig. 2(b) depicts the unfluidized section of the frog sand bed. According to web site http//www.bigai.ne.jp/miwa/sand/what/, the sand grains are composed of 99% quartz and the mixture contains 100 cm^3 of water. The cell is constructed from acrylic resin and the ends are sealed with circular acrylic plates 1 mm thick. The similarity of the case of the frog sand to that of the singing sand, as will be seen later, led to the assumption that the fluidized sand depth $h \approx 1$ cm and thus from Fig. 4, $\beta \approx 1$ mm, where $h/\beta \approx 10$ from Eq. (21). The estimated average grain diameter is close to 0.45 mm. According to published reports (Bagnold 1954; Brown et al., 1964; Shen and Ackermann, 1982), the effect of the water as the interstitial fluid can be neglected. Further, from Eq. (A.21), η in the slip channel is of the order of 1 kg/(m s), while that of water is about thousand times smaller.

Fig. 5 depicts a nearly entire event of an acoustic emission recorded in early January, 2000 at the Exploration Laboratory of the International Nickel Company in Sudbury, Ontario. A piezoelectric film was taped to the cell wall, with a thin layer of regular honey interposed, and the signal was fed into a Tektronix oscilloscope, model TDS42A.

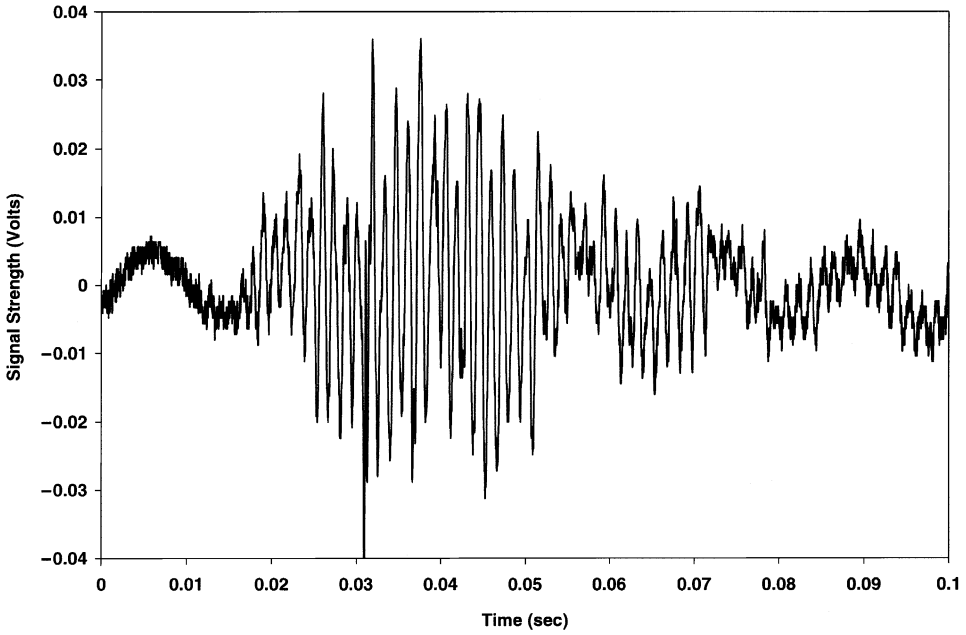

Fig. 5. Time signal from the frog sand, with the cell held in a horizontal position and moved gently back and forth. A piezoelectric film was taped on the cell wall and the signal was stored in a digital oscilloscope. The AC 60 cycle component is clearly discernible.

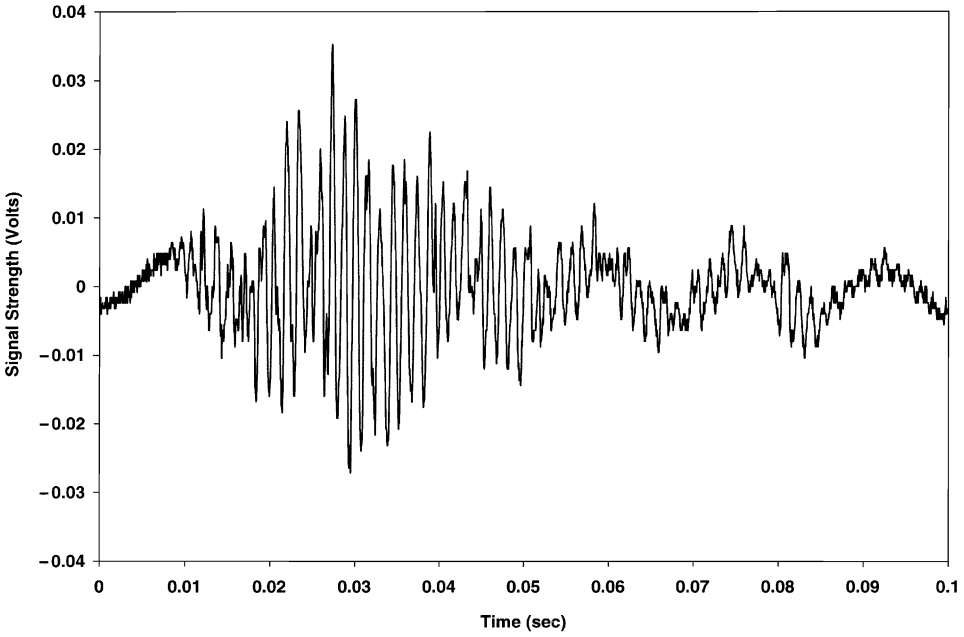

Fig. 6. Same as Fig. 5, but 1 month later.

Fig. 6 depicts a similar signal recorded about 1 month later. Overall, the signals in both cases appear to be the same. However, the frequency components and their strengths differ, as shown in Figs 8 and 9 and in Table 1. Fig. 7 shows five such events separated by about 100 ms. The tactile sensation of about 10 Hz was clearly felt when the signal was emitted. The 60 Hz electric power component can be seen in Figs. 5 and 6 and more so in Fig. 7.

The plots in Figs. 8 and 9 are fast Fourier transforms of the time signals in Figs. 5 and 6, respectively, obtained by the use of the Matlab signal processing toolbox software. The most visible frequencies around the dominant frequency $f_d = 690$ or 689 Hz, are shown in columns 2 and 3 of Table 1. There is no definite pattern in the distribution of these frequencies labeled by the letters a, b, c... on the left of f_d and by a', b', c'... on the right of f_d, except that the average spacing Δf is about 20 Hz. Similar frequency spectra with spacing of about 23 Hz were recorded by Qu et al. (1995).

The near equality of the dominant frequencies in Figs. 8 and 9 is considered to be more of a coincidence than the rule. In both cases, the cell was moved back and forth horizontally rather gently and the signal was recorded soon after the motion began. In the early stages of testing for signal emission and its frequency analysis, the value of $f_d = 603$ Hz was determined. A more vigorous movement of the cell could have resulted in a larger depth h and a larger β and thus in a lower f_d, as seen in Eq. (18) with $V_s = 1$ m/s. A similar change in f_d, from 66 to 53 Hz, is reported in Criswell et al. (1975), regarding the avalanching booming sand. While in most cases the frequency spacing is close to 20 Hz, (Table 1), there are cases where Δf is considerably less or more than 20 Hz. Therefore, these frequency spectra are not merely composed of harmonics of the fundamental equal to 20 Hz.

The method of computation of the eigenfrequencies f_i and the vibration patterns, Eq. (24), was tested on a simple velocity profile comprised of two very deep square wells with a rigid wall on the right and air on the left. Such a velocity profile corresponds, in the low frequency limit, to the familiar two mass–two spring system, where the weightless spring at right is attached to a rigid wall and the blocks of mass M slide without friction on the floor. The system has two degrees of freedom and two natural frequencies of vibration. The lower frequency corresponds to the mode where both blocks move in phase and the higher to the mode where the blocks move out of phase, the ratio of the two frequencies being 2.618. The positions of the wells correspond to those of the springs. It was determined that the ratio of the two lower frequencies is also 2.618. Further, the standard test procedure (Barber and Yeh, 1975; Lapalme and Patitsas, 1993; Noel and Patitsas, 1998) of shifting the origin O' and looking for changes in the frequency spectrum was used in the simple model and in more complex cases, such as the one shown in Fig. 4.

The required parameters in Eq. (24) are listed in Tables 2 and 3 No frequencies could be found until the phase velocity at the middle of the last interval to the left of O', in Fig. 4, was reduced substantially. When the complex phase velocity $V_c(8) = (0.389 \pm j0.388)$ was reduced to $(0.04 \pm j0.0)$, a frequency spectrum was obtained with fundamental $f_o = 33.6$ Hz and overtones beginning with 40.0 Hz, having an average spacing $\Delta f \approx 20.0$ Hz. The irregularity in the

Table 1
Frequency spectra for the frog sand

Peak	Frequency(Hz) Fig. 8	Frequency(Hz) Fig. 9	Frequency(Hz) theoretical
y		139	
w		191	
t	266		
s		258	
o	390	360	
m		422	
l		455	496
j		494	513
i		506	536
h	553		552
g	572	560	571
f		577	593
e	607	598	608
d		628	630
c	641	650	649
b	660	670	665
a	690	689	688
b'	708	709	705
c'	737	721	723
d'	779	744	745
e'		762	761
f'	811	779	781
g'	833	798	802
i'		850	817
n'	1019		839
t'	1187		858

The first column lists the labels of the peaks shown in Figs. 8 and 9 and the second and third columns list the corresponding frequencies. The fourth column lists the theoretically predicted frequencies. Not all peaks in Figs. 8 and 9 are included.

frequency spacing can be attributed to the interaction between the modes in the 8th interval and those in the velocity well at O'. It becomes more pronounced when the relaxation time τ is reduced . It may be noted that the spectrum with $f_o = 20$ Hz and harmonics of f_o corresponds to an infinite square velocity well having width $L = \beta = 1$ mm and $V = 0.04$ m/s. More irregularities in the frequency spectrum can be obtained by reducing the velocity $V_c(7)$. The fourth column in Table 1 is a frequency spectrum computed with $V_c(7)$ reduced from its original value of $(0.808 \pm j0.796)$ to $(0.100 \pm j0.000)$ and $V_c(8)$ from its original value to $(0.060 \pm j0.000)$. For comparison purposes, the phase velocities for $f = 690$ Hz at the middle of the intervals 0, 1, 4, to the left of O', are, respectively, $(2.009 \pm j1.840)$, $(2.024 \pm j1.852)$ and $(4.991 \pm j3.378)$. It cannot be argued that the values $\Delta = 0.5$ and $w_f = 0.5$, in Table 3, are unique. However, the relatively low value of Δ corresponds to the relatively low level of fluidization due to the gentle movement of the cell. The value of w_f is justified further below. In general, the frequency spectrum depends very critically on $V_c(8)$ and weakly on Δ and w_f.

The necessity to reduce the value of $V_c(8)$ could be attributed to the presence of a surface boundary layer. Haff (1983) alluded to such a layer and Thompson (1993), in a computational study, presented a graph showing considerable grain saultation on the surface when the granular bed was driven by a vibrating plate at the bottom of the bed. The critical dependence of the frequencies f_i on the width and the phase velocity of the boundary layer can account for the lack of reproducibility of the spectra, as seen in Table 1 and in Criswell et al. (1975). Further, it will be seen below that the values of $\bar{v}/\Delta u$ and β are history-dependent, rendering the exact reproduction of the frequency spectra very unlikely. In this sense, it could be argued that the lack of acoustic emissions, when slabs of sand in a sand pile break off and slide downhill, has its origin primarily in the insufficient fluidization of the surface boundary layer. In the case of Fig. 3(a), the surface boundary layer is clearly ill-defined and so is the frequency spectrum, according to Fig. 11(c) in Miwa et al. (1983).

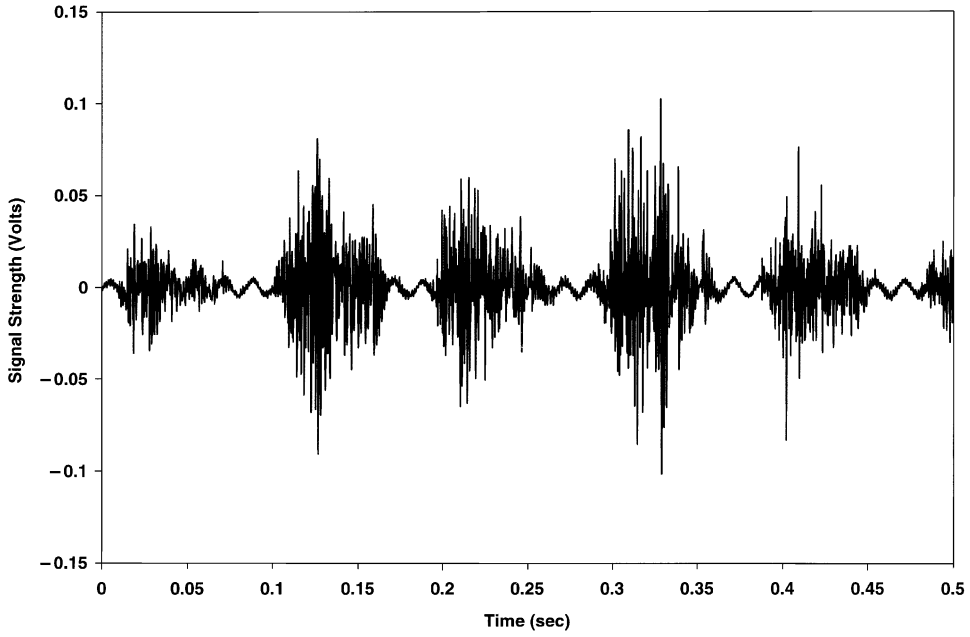

Fig. 7. Same as Fig. 5 but on a longer time scale.

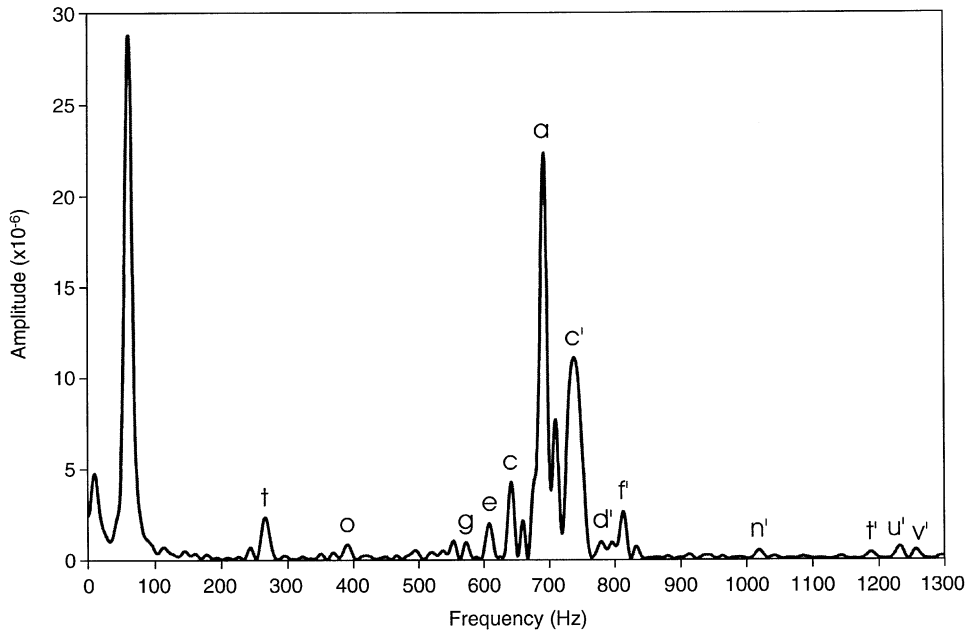

Fig. 8. The frequency spectrum corresponding to the time signal in Fig. 5. The frequencies, enumerated by the Latin letters, are shown in Table 1.

Fig. 10 shows a plot of the real part of the acoustic pressure amplitude p_a versus y/β with $w_f = 0.5$ and $f_d = 690$ Hz. The peak occurs at the middle of the first interval to the left of O', i.e., at $y/\beta = 6.75$. It follows that while the frequency spectrum is principally determined by the properties of the boundary layer, due mainly to the large value of the relaxation time τ in the rest of the grain bed, the energy transfer to the modes of vibration occurs in the slip channel. While the plot remains nearly the same for changes in Δ from 0.5 to 1.0, for example, the value $w_f = 1$ results in a peak

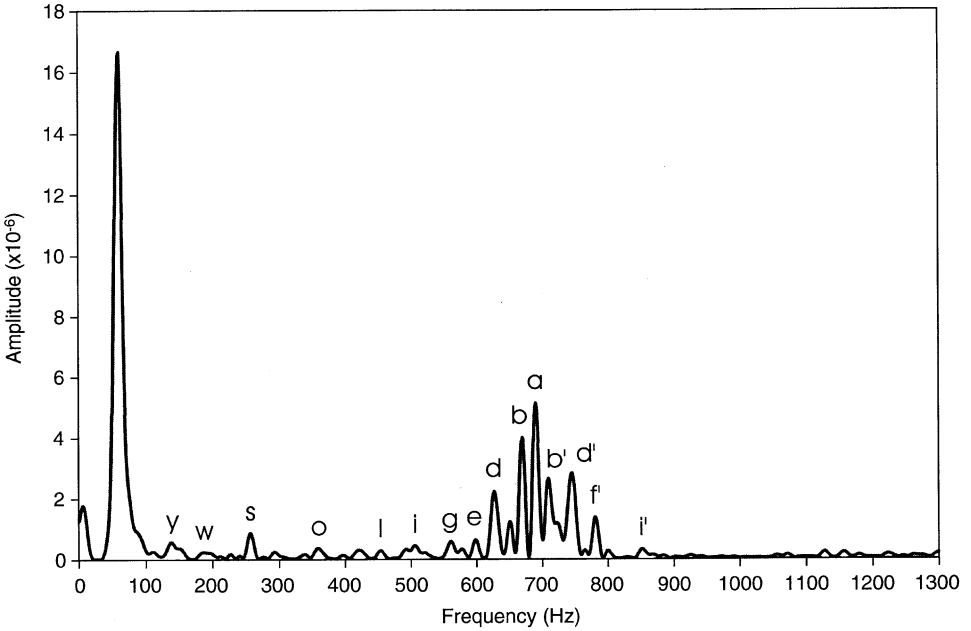

Fig. 9. Same as Fig. 8, but for Fig. 6.

Table 2
Experimental data on the phenomena of the booming–singing sands

Sand type	β (mm)	d (mm)	β/d	$1/\beta$ (1/m)	f_d (Hz)	V_s (m/s)	ψ (deg)
Booming sand (avalanching)	13.0	0.34	38.2	77	66	1.03	32
Booming sand (in glass jar)	4.3	0.34	12.6	232	200	1.03	
Frog sand	1.0	0.45	2.2	1000	690	0.69	
Sonorous sand	4.8	0.50	9.5	208	210	1.00	35
Singing sand	1.0	0.45	2.2	1000	850	0.85	35

β is the fluidization parameter $\approx h/10$, where h is the depth of the fluidized sand bed. β is nearly equal to the slip channel width w. β/d is nearly equal to the number of layers in the slip channel. f_d is the dominant frequency of the acoustic emission. $V_s = 2\beta f_d w_f$ is a measure of the real part of the phase velocity in the slip channel. w_f is a correction factor listed in Table 3. ψ is the angle of dynamic sliding $= \tan^{-1}(\sigma/p)$.

at $y/\beta = 6.5$, which lies near the edge of the slip channel. The value $w_f = 0.5$ for the sonorous sand can be deduced fairly accurately from Fig. 3(a), as outlined in Section 3.2. The plots for the adjacent frequencies $f_b = 670$ Hz and $f_{b'} = 709$ Hz are nearly the same as in Fig. 10, but as f_i becomes more distant from f_d, the peak moves further away from the center of the channel. There is no apparent reason why the modes corresponding to two adjacent frequencies are not equally excited. The plot with $f = 343$ Hz peaks asymmetrically at $y/\beta = 6.5$ and then decreases monotonically for larger y/β, while the plot for $f = 41.3$ Hz has one oscillation between $y/\beta = 0$ and 2.0 and then it increases monotonically for larger y/β. When the relaxation time τ is reduced by a factor of 100, the plot for $f_i = f_d = 690$ Hz assumes the form of a cosine function, with wavelength equal to β, centered at O'.

3.1.2. *Avalanching booming sand*

In the case of the avalanching booming sand, the only known quantitative study is that by Criswell et al. (1975). The recorded time signals have the overall appearance of those in Figs. 5 and 6. The dominant frequency in Fig. 4(d) in Criswell et al. (1975) is 66 Hz surrounded by 58, 61, 68, 72, 76 Hz and appreciable 'overtones' at about 120 Hz, the

Table 3
Computed parameters for the five cases listed in Table 2

Sand type	q_2	Δ	w_f	$\bar{v}_o$ (cm/s)	λ_B	$\bar{v}/\Delta u$	μ	e	Δu (cm/s)
Booming sand (avalanching)	0.79	0.8	0.6	49.0	5.2	19.5	0.600	0.875	2.0
Booming sand (In glass jar)	0.83	0.8	0.6	19.1	13.0	12.7	0.550	0.850	1.2
Frog sand	0.87	0.5	0.5	8.3	13.3	5.2	0.67	0.900	1.0
Sonorous sand	0.77	0.5	0.5	27.4	5.8	16.2	0.670	0.800	1.3
Singing sand	0.87	0.5	0.5	6.7	15.5	5.2	0.670	0.900	1.0

q_2 is the factor in the equation of state (A.16). Δ is the measure of the work done by the slip channel on the overburden during delatancy, Eq. (15). $\bar{v}_o$ is the fluctuation velocity given by Eq. (22), which is higher by 20% than the fluctuation velocity at the center of the slip channel for the case of Eq. (19a). λ_B is the Bagnold linear concentration parameter and $\bar{v}/\Delta u$ is the velocity ratio characteristic of the state of the grain bed. μ and e are the coefficients of friction and restitution, respectively, and Δu is equal to the entry in column 5, reduced by 20%, then divided by the entry in column 7. Its value of 2 cm/s, in the case of the booming avalanching sand, could be closer to 1 cm/s, as outlined in Section 3.2.

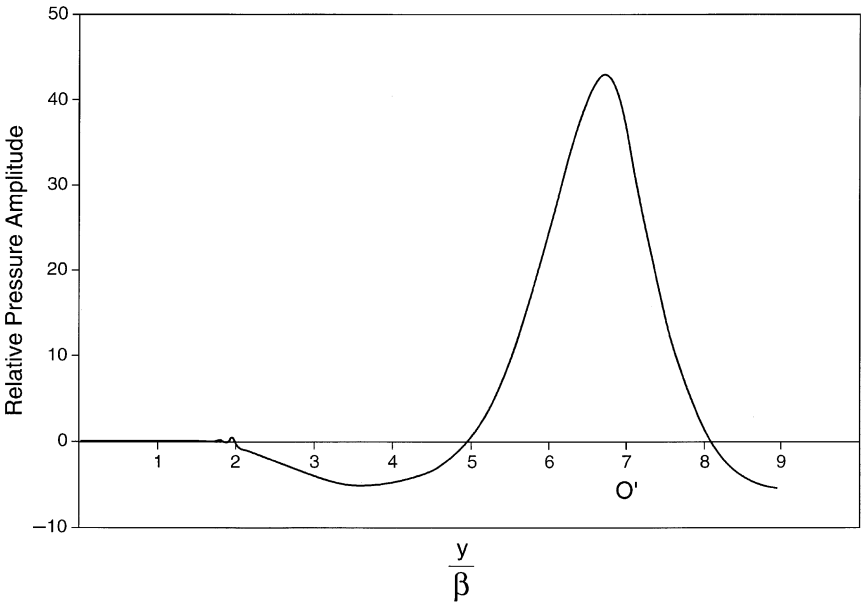

Fig. 10. Plot of the real part of the relative pressure amplitude p_a versus y/β, Fig. 4, for the case of the frog sand. The relevant parameters are: $f_d = 690$ Hz, $\Delta = 0.5$ and $w_f = 0.5$.

average spacing being 3.6 Hz. As in the previous case, it was necessary to reduce the values of $V_c(7)$ and $V_c(8)$ to $(0.900 \pm j0.400)$ and $(0.09 \pm j0.000)$ respectively in order to obtain the following spectrum: 61, 63, 66, 69, 72 and 75 Hz, with $\Delta = 0.8$ and $w_f = 0.6$. In the case of avalanching snow, the regions of weakness begin as regions of crystallization, which become regions of fluidization when avalanching begins. The assumed absence of acoustic emissions could be attributed to the lack of an appropriate surface boundary layer.

3.2. Analysis of experimental results

Table 2 presents the available experimental data on the five cases where the value of β can be estimated with a sufficient degree of confidence. The value of the angle of sliding, ψ, Fig. 2(a) and Eq. (A.19), was reported reliably only in the case of the avalanching sand (Lindsay et al., 1976), while from Miwa et al. (1983) it can be inferred that it is close

to 35° for the sonorous and the singing sands. Since the parameters e, μ, $\Delta u/\bar{v}$ are not known, the value of β was obtained from the estimated value of the fluidized granular bed, h, instead of Eq. (12). For only one slip channel, $h \approx (7\pi/2)\beta$ in the case of the singing sand, Eq. (17), and $h \approx 10\beta$ in the cases of the avalanching and frog sands, Eq. (21). In the case of the avalanching booming sand at the Sand Mountain in Nevada, USA, the value of h was reported to be around 13 cm (Criswell et al., 1975; Lindsay et al., 1976). In the case of the same booming sand in a glass coffee jar, 8 cm in diameter by 16 cm in height, it was determined that the sound emission ceased when the sand depth was reduced to between 4 and 4.5 cm, implying a value of β close to 4.3 mm. In the case of the singing sand, the estimation of h was more difficult. When singing sand from the east shore of Lake Michigan, USA, was in good singing condition, it maintained its singability when sheared gently to a depth of about 1 cm, as shown in Fig. 1. Further, the data shown in Figs. 2 and 4 in Nishiyama and Mori (1982) were obtained for a sand depth of about 1 cm. A reasonable value of the error in the listed values of β could be as high as 20%. The values of the average grain diameter d and the dominant frequency f_d were obtained from Criswell et al. (1975), Miwa et al. (1983), Leach and Rubin (1990), Leach and Chartrand (1994), Qu et al. (1995) and Section 3.1.

The striking features in Table 2 are that the values of $1/\beta$ are close to the values of f_d and that the value of the phase velocity V_s is close to 1 m/s, over a wide range of values of β and f_d. The width factor w_f for the booming sand in the glass jar was assigned the value 0.6, as for the avalanching booming sand, and that for the other sands was assigned the value 0.5, as for the frog sand. These values are listed in Table 3. Evidently, more experimental data on the depth and width of slip channels are needed. It follows from Eqs. (12) and (18) that f_d varies inversely with d, while according to Bagnold (1966) it varies inversely with $\sqrt{d}$. The experimental report by Leach and Rubin (1990) suggests a variation like $d^{-\gamma}$, with γ closer to 1 than 0.5.

From Eqs. (A.16c) and (17), the Bagnold linear concentration parameter $\lambda_B = d/s$ at the center of the slip channel can be written as

$$\lambda_B = \left(\frac{3}{q_2}\right)^{1/2}(1+\Delta)\frac{V_s}{\bar{v}_o} \quad \text{or} \quad \lambda_B = 3\rho(1+\Delta)^2\frac{V_s^2}{p_o}. \tag{25}$$

Similarly, from Eqs. (A.16c) and (22), in the case of the avalanching booming sand

$$\lambda_B = 3\rho(0.3+\Delta)^2\frac{V_s^2}{p}, \quad p = 7\beta\rho g. \tag{26}$$

With $g = 9.8\cos(30^\circ)$, $\Delta = 0.8$ and $w_f = 0.6$, $\lambda_B = 5.2$, in the case of the avalanching booming sand, while $\lambda_B = 13.0$, in the case of the booming sand in the glass jar. In the case of the frog sand, $\lambda_B = 13.3$. A more explicit expression for λ_B can be obtained by using Eq. (12) in Eq. (26), i.e.,

$$\lambda_B = \frac{3}{7}(0.3+\Delta)^2 V_s^2\sqrt{2}\,\frac{(q_1(\Delta u/\bar{v}) - \Gamma)^{1/2}}{gd}. \tag{27}$$

In Fig. 3(a), the slip channels are not formed under the plunger. Therefore, sufficiently away from the plunger, Eq. (26) is more likely to apply than Eq. (25). Effectively, the diagram in Fig. 1 serves mathematical simplicity rather than reality. The distance between the channels, Δs, in Fig. 3(a) is estimated to be 30 mm, the width of the plunger having been reported to be 30 mm, in a private communication with Shigeo Miwa. With $\Delta s/\beta = 2\pi$, it follows that $\beta = 4.8$ mm. Further, the ratio $\Delta s/w$ is estimated to be 6, on average, resulting in channel width $w = 5$ mm and $w_f \approx 0.5$. In the case of the sonorous sand with $\Delta = 0.5$, $\lambda_B = 5.8$, while in the case of the singing sand $\lambda_B = 15.5$. Slightly larger values of Δ result in unacceptably large values of λ_B, i.e., $\lambda_B \gg 17$. This puts in question the validity of the equations of fluid mechanics in the present context and the assumptions leading to Eq. (26), regarding the existence of modes of vibration in the sand beds. However, the relatively narrow range of the allowed values of Δ could reflect the rarity of these phenomena. For example, relatively large values of Δ tend to reduce the depth of the velocity well in Fig. 4, and consequently to reduce the intensity of the acoustic emissions.

The angle θ_o appearing in the integrals defining the constants I_{ij} in Eq. (A.14) increases with grain separation. If θ_o is 30° when $s/d = 0$ and 60° when $s/d = \frac{1}{2}$, the following simple relation can be used

$$\theta_o = 30 + 60\,\frac{1}{\lambda_B}. \tag{28}$$

However, the precise value of θ_o is not critical in the relevant computations. Fig. 11 shows plots of β/d and of λ_B versus $\bar{v}/\Delta u$ based on Eqs. (12) and (27), respectively with $\mu = 0.500$, $e = 0.850$, $\Delta = 0.6$ and $V_s = 1$. At $\bar{v}/\Delta u \approx 11.2$, $(\beta/d)^2$ changes sign and thus for $\bar{v}/\Delta u > 11.2$, β/d is equal to the value shown in Fig. 11, multiplied by $\mathrm{j} = \sqrt{-1}$. The value of $\bar{v}/\Delta u = \bar{v}/\Delta u|_o$, at which the change of sign occurs, decreases strongly with decreasing μ and especially so with decreasing e. The plot of λ_B for $\bar{v}/\Delta u > 11.2$ is questionable since there is no slip channel for these values of the velocity

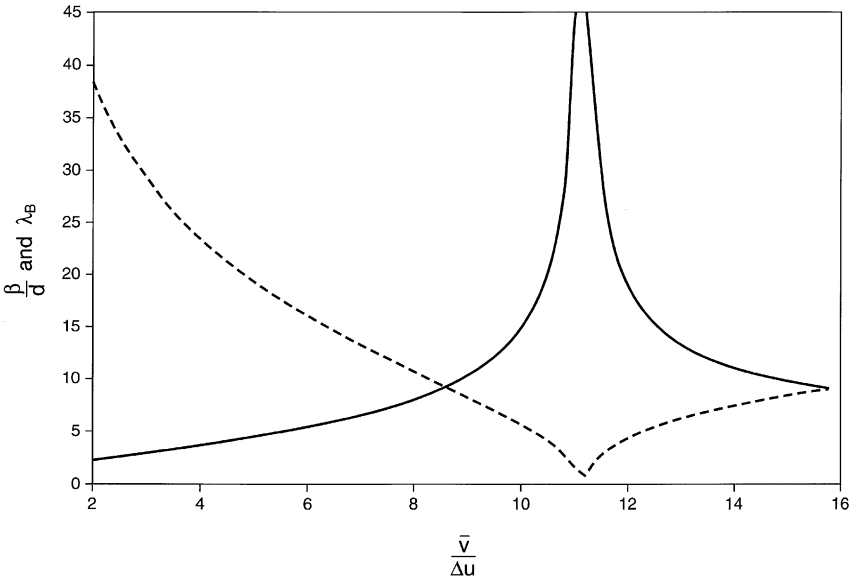

Fig. 11. Plots of β/d, Eq. (12), solid line and of $\lambda_B = d/s$, Eq. (27), broken line, versus the velocity ratio $\bar{v}/\Delta u$ for: $\mu = 0.5$, $e = 0.85$, $\Delta = 0.6$ and $V_s = 1$ m/s. For $\bar{v}/\Delta u > \bar{v}/\Delta u|_o = 11.2$, where $\beta/d \to \infty$, the value of β/d shown has to be multiplied by $\sqrt{-1}$. Further, the part of the plot with $\lambda_B < 5$, about, is not applicable since Eqs. (A.16a)–(A.16c) are not applicable when $s \to d$.

ratio. However, even in an unsingable grain bed it could be argued that larger β, i.e., larger fluidization, implies smaller λ_B. Further, in the neighborhood of $\bar{v}/\Delta u|_o$, where λ_B is smaller than about 5, the plot for λ_B cannot be expected to apply since Eqs. (A.16a)–(A.16c) cannot be expected to apply to a relatively loosely compacted granular bed.

Fig. 12 shows plots of e versus μ obtained from Eq. (12) with $d/\beta = 0$ for various values of $\bar{v}/\Delta u|_o$. The value of θ_o was computed with $\lambda_B = 10$. The plot with $\bar{v}/\Delta u|_o = 20$ lies just below that with $\bar{v}/\Delta u|_o = 30$ and those with $\bar{v}/\Delta u|_o > 30$ practically coincide with it. The plots with $\lambda_B = 5$ lie slightly above those with $\lambda_B = 10$. It follows that for given μ and e, the granular bed is unsingable if $\bar{v}/\Delta u > \bar{v}/\Delta u|_o$. It will be argued in Section 3.3 that the ratio $\bar{v}/\Delta u$ can be altered by modifying the confinement of the granular bed.

From reports in Lewis (1936), Lindsay et al. (1976) and Haff (1986), it is estimated that in the case of the avalanching booming sand, the overburden avalanches with a velocity close to 20 cm/s. With the effective channel width w approximately equal to β and with $d = 0.34$ mm, it follows that there are 44 sliding layers in the channel, resulting in an average $\Delta u = 0.45$ cm/s. However, from Fig. 14(b), Δu could be several times larger than this value during the acoustic emission. It will be argued in Section 3.4 that the acoustic emission takes place during the latter phase of the delatancy stage, corresponding to the latter part of the interval CD in Fig. 14(b). The use of the parameters, shown in Table 3, in Eq. (22) results in $\bar{v}_o = 49.0$ cm/s and in $\bar{v} = 39$ cm/s at the center of the slip channel, according to Eq. (19). In the absence of any other information on Δu, the value of 2 cm/s was assumed, resulting in $\bar{v}/\Delta u = 19.5$. Using the values of λ_B and ψ given in Tables 2 and 3, μ was determined from Eq. (A.19). Then e was varied in Eq. (12) until the value of $\beta/d = 38.2$ was obtained. The procedure resulted in the unique values $\mu = 0.600$ and $e = 0.875$.

It can be seen in Fig. 12 that the doubling of the value of $\bar{v}/\Delta u$ results in a minute increase in the value of e, implying that knowledge of the precise value of Δu is not essential. For example, the values $\mu = 0.62$ and $\Delta u = 1.5$ cm/s result in $e = 0.900$. In general, the value of μ is 5–10% lower than $\tan\psi$. The relatively large value of β/d implies that $\bar{v}/\Delta u$ is just under $\bar{v}/\Delta u|_o$. Therefore, a slight increase in the air humidity can result in a thicker water coating on the grains and thus in lower values of μ and e, rendering the sand unboomable. This could be one reason why the booming sand phenomena are more rare than the singing sand phenomena where β/d is relatively small. Further, according to Section 3.4, the excess moisture on the grain surface could alter the surface texture, rendering the granular bed unboomable by reducing the level of excitation of the elastic modes in the grains.

In the case of an unsingable granular bed with $\bar{v}/\Delta u \gg \bar{v}/\Delta u|_o$, β/d approaches Γ^{-1}, implying a small β unless $\Gamma \to 0$. Further, as $\bar{v}/\Delta u \to \infty$, $\Delta u \to 0$ in a non hyper-fluidized granular bed, resulting in $\eta \to \infty$ from Eq. (A.21). It follows that such a state could describe a highly compacted sand bed. Similarly, with $\bar{v}/\Delta u \to \bar{v}/\Delta u|_o$ from either side in Fig. 11, β becomes very large, and with $\bar{v}/\Delta u \to 1$, Δu becomes very large in a hyper-fluidized sand bed, implying a small viscosity η. Such a state could describe a bed of dry quicksand.

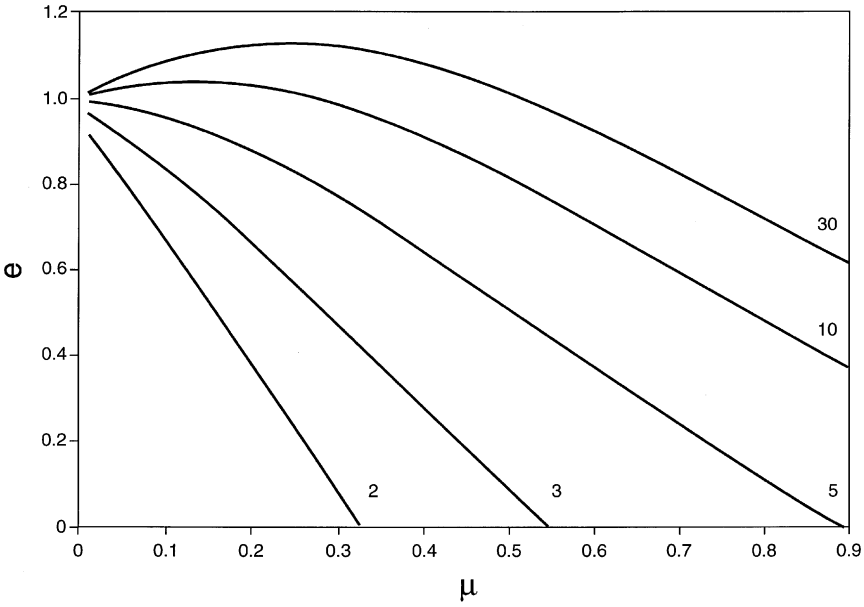

Fig. 12. Plots of e versus μ, based on Eq. (12) with $d/\beta = 0$, for various values of $\bar{v}/\Delta u|_o$. The plots with $\bar{v}/\Delta u|_o > 30$ practically coincide with the plot for $\bar{v}/\Delta u|_o = 30$. The rise of this plot above 1.0, for low values of μ, can be attributed to the inadequacy of Eq. (A.8) regarding the interruption of the sliding during collision.

In order to obtain a measure of the value of the coefficient of restitution of the singing sand, approximately 2000 grains of singing sand from Lake Michigan, of booming and silent sands and glass beads of comparable size were dropped and tumbled in a stainless-steel cooking pot 25 cm in diameter by 10 cm in depth. It was observed that the grains from the booming and silent sands rebounded somewhat less than those from the singing sand and the glass beads. Since e for glass is known to be in the neighborhood of 0.9 (Goldsmith, 1952), the same value is shown in Table 3 for the singing sand.

In the case of the booming sand in a glass jar, $\bar{v}/\Delta u$ and ψ are not known. Thus, the unique determination of μ and e is not possible. However, the relatively more humid conditions in Sudbury compared to those at the Sand Mountain could result in somewhat lower values for these parameters. The values shown in Table 3 with $\bar{v}/\Delta u = 12.7$ result in $\beta/d = 12.6$, shown in Table 2, but the values 0.500 and 0.875 could also be used. In the case of the sonorous sand, μ was chosen to be 0.67 in order for ψ to be near 35°. Then, the values of e and $\bar{v}/\Delta u$, shown in Table 3, result fairly uniquely in the value of β/d shown in Table 2. In the case of the singing sand, the values $\mu = 0.670$, $e = 0.900$ and $\beta/d = 2.2$ result in $\bar{v}/\Delta u = 5.2$. In the case of the frog sand, there is not sufficient information to determine the values of q_2, μ and e. However, its similarity to the singing sand, in geometry and acoustic emission, suggests that these parameters ought to have values close to those of the singing sand. From Fig. 7, the duration of an entire acoustic emission is somewhat longer than 0.5 s. With $\Delta u = 1$ cm/s and two layers in the slip channel, the displacement of the overburden amounts to about 1 cm. Such a displacement does not contradict the visual perception of the sand movement when the acoustic emission takes place.

From reports in Miwa et al. (1983) and the tumbling of common sand grains in the cooking pot, it follows that the values of μ and e are not appreciably different from those of the singing sand, which has $\bar{v}/\Delta u = 5.2$ and $\bar{v}/\Delta u|_o \approx 170$. It follows that common or ordinary sand beds are potentially singable, but silent because they are characterized by relatively very low ratios $\bar{v}/\Delta u$, to the point where β and w are smaller than d.

The values of Δu in Table 3 lie well below the value of $\sqrt{gd} = 7$ cm/s with $d = 0.5$ mm. Above this value, the granular bed could be described by ideas drawn from the kinetic theory of gases, according to Thompson (1993). In the context of the kinetic theory of gases, η is proportional to Δu for fixed λ_B, while from Eq. (A.21) it is nearly proportional to $1/\Delta u$ for fixed pressure p. Therefore, for some value Δu_c between 2 and 7 cm/s, η could acquire a minimum value.

In the case of the avalanching booming sand with $\bar{v}_o = 49.0$ cm/s, $\Delta u = 2$ cm/s, $d = 0.34$ mm and $\lambda_B = 5.2$, it takes 17 ms for one grain to overtake another and there are about 64 collisions between the two grains in the process. With a signal time of about 600 ms (Criswell et al., 1975), there are 35 overtakings during one acoustic event. In the case of the

frog sand with $\Delta u = 1.0\,\mathrm{cm/s}$ and $d = 0.45\,\mathrm{mm}$, the overtake time is 20 ms. From Figs. 5 and 6, the signal time is about 80 ms, resulting in only two overtakings during one event.

Eq. (27) was derived for a fluidized granular system inside a slip channel. However, apart from the stick–slip dissipation parameter Δ, the other parameters, namely μ, e, $\bar{v}/\Delta u$ and V_s can also characterize any fluidized granular bed, which is not necessarily singable. Therefore, it is cautiously proposed that Eq. (27) be used in all such cases with $\Delta \approx 0$. In the experimental report by Savage (1978), glass beads 1.8 mm in diameter were sheared in an annular cell having width $h = 3.8\,\mathrm{cm}$ and mean radius $\bar{r} = 12.7\,\mathrm{cm}$. The upper and lower walls were lined with coarse sand paper and the side wall was smooth. With $\lambda_B = 9.5$ and mean shear rate $\omega\bar{r}/h = 50\,\mathrm{s}^{-1}$, ω being the angular velocity of the disk, the ratio of the shear stress to the normal stress is estimated to be about 0.45, from Fig. 12 in Savage (1978). This implies $\mu \approx 0.4$, which lies in the range of μ for glass on glass (Shand, 1958). The mean velocity U of the rotating disk is $\omega\bar{r} = 1.9\,\mathrm{m/s}$ and with 21 layers in the glass bed, $\Delta u = 9\,\mathrm{cm/s}$, assuming a constant relative velocity gradient throughout. However, Δu could be much smaller if a boundary layer were assumed to exist on the surface of the disk. If $\bar{v} = U$, then $\bar{v}/\Delta u$ is greater than 21. In Fig. 12, the point with $\mu = 0.4$ and $e = 0.9$ lies on the curve with $\bar{v}/\Delta u|_o = 10$, implying that the granular bed is not singable. With $\rho = 1700\,\mathrm{kg/m^3}$, $\Delta = 0$, $V_s = 1\,\mathrm{m/s}$ and $p_o = 1000\,\mathrm{N/m^2}$, $\lambda_B = 5.1$, from Eq. (25). However, λ_B is close to 9.5 with $\Delta = 0.4$.

3.3. Squeezed grains

In the experimental study by Nishiyama and Mori (1982), several plots of f_d versus μ_r, the reduced mass of the rod and the mortar, are included, for various singing sands and also for glass beads 0.6 mm in diameter placed in a mortar with about 1 cm bed thickness. In Fig. 4 in that report, the dominant frequency of the acoustic emission, f_d, decreases nearly as the inverse of $\sqrt{\mu_r}$. The authors interpreted this functional dependence of f_d on μ_r as the result of the sand mass (under the rod) acting as a short spring, or an elastic bar, between the rod and the mortar. The system can be simulated by an elastic bar, characterized by mass M_b, length L and phase velocity V_s, attached to a rigid wall at one end and to a rigid block of mass M at the other end. It follows that V_s exceeds the values listed in Table 2 by a factor of more than 10, when the fundamental mode is considered with $L = 5\,\mathrm{mm}$ and $f_d = 2000\,\mathrm{Hz}$. In the context of this study, the decrease of f_d with the mass of the plunger can be attributed to the increase of β and λ with increasing p, according to Eq. (26).

In order to establish that the sand directly under the rod could not be responsible for the sound emission, singing sand, about 1 cm deep, was placed in a plastic cylindrical pill-cell having inner diameter and height equal to 2 and 5 cm, respectively. The sand was then impacted by a cylindrical rod, which could barely slide inside the pill-cell. The sand reacted like a solid mass without any musical acoustic emission. However, when it was impacted by a brass pestle, 8 cm long and tapered to a maximum diameter of 1.1 cm at the larger end, the acoustic emission with f_d close to 1000 Hz was readily produced. This simple experiment clearly demonstrates that the motive force towards the fluidization of the sand bed is the relative flow velocity Δu, and that the musical acoustic emission requires grain flow. Upon impaction, the sand in the mortar becomes fluidized and a region of failure is established around the rod. When the rod is close to the floor of the mortar, the pressure p_o, in Fig. 1, becomes sufficiently large to push the sand in the region of failure, and that above it, towards the region of lower pressure.

In order to eliminate, as much as possible, the excitation of modes of vibration associated with the mortar, about 250 ml of singing sand from Lake Michigan was placed on a cotton cloth at the bottom of a plastic bowl of diameter equal to 18 cm. The pile was flattened out to a bed depth of about 2 cm. After impacting the bed lightly at the same point several times with a plunger 2 cm in diameter, a depression was formed with depth at the center close to 0.7 cm and diameter at the rim close to 5 cm. A better acoustic emission was obtained when the plunger, held at about 30° from the vertical, impacted the sand about 1 cm from and directed towards the centre. Although the sound was invariably heard, the quality of the signal on the oscilloscope screen depended significantly on the speed of impaction and the type of plunger.

Fig. 13(a) shows one of the better signals when the plunger was a relatively smooth rock 5 cm long and 3 cm at its widest diameter. The impacting end had a radius of curvature of about 1 cm. There are close to 13 oscillations in the 10 ms time span, resulting in $f_d = 1300\,\mathrm{Hz}$. With $V_s = 1\,\mathrm{m/s}$, it follows that $\beta = V_s/f_d = 0.77\,\mathrm{mm}$ and $h_s = 7\beta = 5.4\,\mathrm{mm}$, i.e., the slip channel lies about 5.5 mm below the sloping surface of the depression. Only one acoustic event was observed during one impaction, lasting about 50 ms. When the cylindrical rod impacted the sand near the center of the depression, an appreciable sand mass near the top of the depression could be seen to collapse downwards, and more sand collapsed downwards to fill the space occupied by the rod when it was removed. Yet, after several such impactions the geometry of the depression remained nearly the same, implying that the sand mass was displaced upwards by some mechanism.

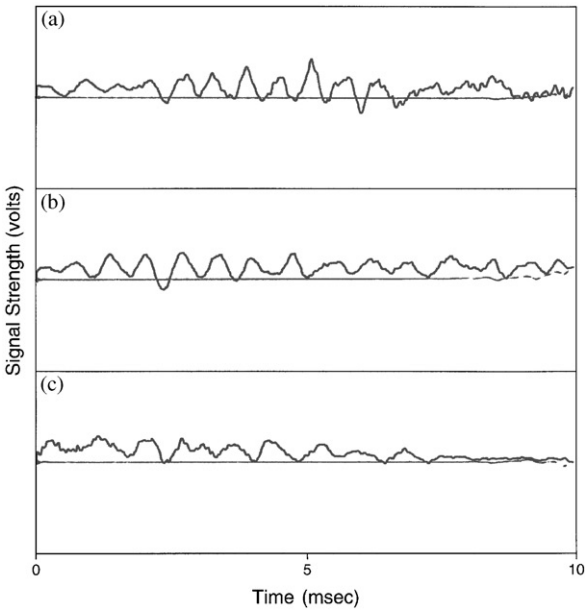

Fig. 13. (a) Time signal after several light impactions at the same point on an approximately 2 cm deep by 20 cm in diameter pile of nearly silent sand from Lake Michigan placed on a hard surface. The final depression had depth of about 0.7 cm at the center and diameter of about 5 cm at the top. (b) Same as part (a) with an otherwise silent beach sand, $d \approx 0.4$ mm. (c) Same as part (a) with a coarser, nearly silent sand placed on a 2.5 cm thick foam pad.

Fig. 13(b) shows a similar recording using an otherwise silent beach sand from the village of Providence Bay on the south shore of Manitoulin Island, west of Sudbury, Ontario. There are 14 oscillations, resulting in $f_d = 1400$ Hz. The plunger was the small brass pestle and the grain size was close to 0.4 mm. In order to establish that the sound emission was not due to air mass oscillations, as when two rock surfaces are rubbed together, or due to surface wave excitations, the sand pile was placed on a cotton cloth, which was placed on a soft foam pad 2.5 cm thick. For the two cases discussed above, it was not possible to produce a clear signal on the oscilloscope. However, with sand from a beach south of the village of Agios Petros near the village of Vasiliki, Lefkada, Greece, the signal shown in Fig. 13(c) was obtained using the rock plunger. This sand is fairly coarse, about 0.6 mm in diameter and exhibits relatively little resistance to the impacting plunger, similarly to glass beads (Brown et al., 1964). It is acoustically relatively weak when shaken in a glass jar. A similar signal could be obtained using common table salt. Similar signals could be obtained using piles, in the plastic bowl or on a sheet of plywood 1.5 cm thick, composed of grains of booming sand, a fine silent sand used for anti-skid purposes, table salt and common white sugar. Better signals could be heard by placing the piles on a glass pane 45×50 cm in size and 7 mm thick. Similar acoustic emissions could be heard when the above-mentioned grains were placed in the plastic pill-cell to a depth of about 2 cm and impacted by the small brass pestle.

The pan-fried singing sand, prepared by Haff (1986), exhibited the sonorous property when lightly sheared by a spoon, and the nearly silent sand, heated in an oven to about 200°C by Lewis (1936), roared even when picked up in the hands. A few years ago, the singing sand from Lake Michigan sang readily when sheared gently in a dish, regardless of sand depth. Presently, it sings weakly only when forced to flow between the impacting plunger and a rather hard surface, and the common antiskid sand requires a relatively high plunger velocity to become sonorous. In the case of the squeaky sand, a nearly silent singing sand, it was reported by Miwa et al. (1983) that the weak acoustic emission occurred when a relatively large load was placed on the plunger. Evidently, when the grain bed is highly singable the velocity ratio $\bar{v}/\Delta u$ acquires the value of about 5 with only a slight applied shear stress. It will be argued below that the weak singability of a grain bed is most likely due to a very low value of the velocity ratio, which could be increased by the application of a larger shear stress on the grains, in a more confined geometry.

In the experimental study by Brown et al. (1964), glass beads with $d = 0.18$ mm were struck by a cylindrical pestle of 4.3 cm diameter in a dish of 5.0 cm inner diameter. An acoustic emission, described as a shrill, was recorded having a broad-frequency spectrum with a peak at about 3000 Hz. Apart from excitations of the modes of vibration in the dish, the sound emission could be attributed to a slip channel in the gap between the two cylindrical boundaries. From the relation $h/\beta = 7\pi/2$, it follows that $\beta = 0.32$ mm, assuming that the sand depth is equal to the gap between the two

cylindrical boundaries. Further, with $w_f = 0.5$, V_s is equal to 0.96 m/s, which compares well with the entries in Table 2. The number of slip layers is close to $\beta/d \approx 2$.

Takahara (1973) placed grains of singing sand from Kotobikihama in Kyoto prefecture, Japan and rounded glass particles (40 mesh) in a (steel) cylinder of inside diameter and depth equal to 3.5 and 55 cm, respectively, and drove a cylindrical (steel) rod of diameter equal to 2.5 cm into the sand column with a relatively large load of 28.12 kg. The frequencies f_d for the two cases are estimated to be 330 and 220 Hz respectively. With $h = 0.5$ cm, $\beta = 0.45$ mm, resulting in $V_s = 0.15$ and 0.09 m/s for the singing sand and the glass grains respectively. The grain diameter in both cases is close to 0.4 mm, implying only one slip layer. It may be concluded that when the grain bed is hyper-fluidized, V_s can acquire values appreciably below 1 m/s.

Brown et al. (1964) reported that when glass beads of diameter 0.18 mm were placed in a dish and struck with a pestle, no resistance to the movement of the pestle through the grains could be felt and no note was produced. It was established by this author and also reported by Sholtz et al. (1997) that booming sands also remain silent when placed in a relatively large deep dish and sheared on the surface, and that singing sands remain silent when induced to avalanche on an inclined plane. However, in the case of the booming sand from the Sand Mountain, considerable resistance to the movement of the pestle can be felt. In the case of the glass beads, where μ is relatively low and e is relatively high, $\bar{v}/\Delta u|_o$ is considerably larger than 30, according to Fig. 12. Therefore, the grain bed is silent because $\bar{v}/\Delta u$ is relatively very low, resulting in a highly energized surface boundary layer, as in Fig. 3(b). If $\bar{v}/\Delta u > \bar{v}/\Delta u|_o$, then in the process of decreasing the bed depth to about 1 cm, there would be a transition from unsingability to singability accompanied by a very low frequency emission. The absence of such a transition implies that all such grain beds are potentially singable.

While table salt flows similarly to a regular liquid, the fine antiskid sand flows similarly to the avalanching booming sands (Lewis, 1936; Criswell et al., 1975; Lindsay et al., 1976; Nori et al., 1997). That is, when about 500 ml of sand is placed in a dish and tilted sufficiently, plate-like slabs ranging in thickness from about 5–10 mm break off and slide downwards. In the former case, it could be argued that the granular bed is intrinsically unboomable, while in the latter case, it could be argued that $\bar{v}/\Delta u$ is relatively small, resulting in relatively small channel depth h_s. The lack of acoustic emission could be attributed to the instability and non-uniformity of the slip channel, but more likely to the lack of a sufficiently fluidized surface boundary layer. It has been observed that the singability of the singing and booming sands is considerably reduced when they are shaken in a plastic rather than in a glass jar. It may be concluded that the rigidity and the surface texture of the wall of the plastic jar result in a lower value of the velocity ratio $\bar{v}/\Delta u$ compared to that in the glass jar.

3.4. Stick-slip effects

Fig. 7 shows five acoustic events from the frog sand in the interval of nearly 500 ms, each event lasting about 80 ms. In Fig. 1(b) in Nishiyama and Mori (1982), interruption occurs about every 4 cycles in a signal with $f_d \approx 1200$ Hz. From Figs. 6 and 7 in Criswell et al. (1975), it follows that the time between two events is about 750 ms and that the duration of an event is close to 600 ms. The low frequency of interruption, about 1 Hz, of the sound emitted during booming events was reported by (Humphries, 1966) and accounts for the name 'booming' (Sholtz et al., 1997). Although the time interval between events is fairly constant in Fig. 7, in the report by Takahara (1973) it varies from 50 to 150 ms. Therefore, modes of vibration traveling along the slip channel could not be the cause of the interruption of the acoustic emission. The most probable cause appears to be the stick–slip effect known to occur in granular media at relatively low flow velocity rates, Δu (Thompson and Grest, 1992; Thompson, 1993). Thompson and Grest argued that stick-slip effects are associated with compactness and delatancy transitions. Jaeger and Nagel (1992) discussed the relation of the stick–slip effect to the hysteresis effect in the relation of Δu to the angle of repose in a pile of granular material.

In the context of the subject of the singing sands, the stick-slip effect is seen in Fig. 9 in Miwa et al. (1983), where the depth of penetration of the plunger into the sand is plotted versus the force experienced by the plunger. Fig. 14(a) is a sketch of this figure with the axes interchanged in order to correspond to Fig. 7 in Thompson and Grest (1992). The broken line corresponds to the case of the silent sand and the solid line to the case of the sonorous sand. In the plot by Miwa et al. (1983), the points C and C' are roughly half as far from the broken line for the case of the squeaky sand, a nearly silent sand. It follows that the extent of the stick–slip effect determines, in part, the extent of the intensity and the duration of the acoustic emission.

Fig. 14(b) depicts a hypothetical hysteresis loop, which was drawn to account for the stick-slip plot depicted in Fig. 14(a). The point C corresponds to the onset of the slip channels and of the surface boundary layer, facilitating the flow of the sand. It accounts for the collapse of the resistance of the sand to the plunger, depicted by the intervals CD and DA'. The slope $\bar{v}/\Delta u = 5$ of the interval CD corresponds to the case of the singing sand. It is estimated that the acoustic emission takes place during the latter part of the interval CD, where λ_B is relatively small. At point C, Δ tends to be large since λ_B is relatively large, Eq. (27). In turn, a large Δ tends to reduce the depth of the velocity well in Fig. 4,

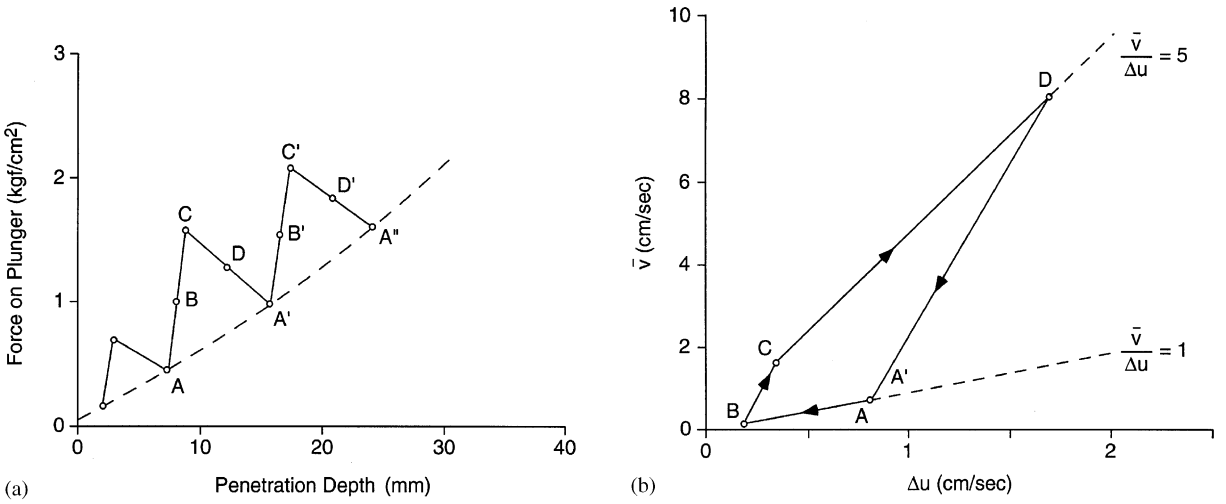

Fig. 14. (a) Rough sketch of the force experienced by the plunger versus penetration depth in a bed of sonorous sand for an experimental arrangement similar to that shown in Fig. 3, based on Fig. 9 in Miwa et al. (1983). The broken line corresponds to a silent sand. (b) A hypothetical hysteresis loop of $\bar{v}$ versus Δu, corresponding to the plot in part (a). The lengths of the various intervals are not necessarily analogous to the lengths of the corresponding time intervals. The slopes $\bar{v}/\Delta u = 5$ and 1 correspond to the singing and silent sands, respectively. The intervals AB and CD correspond to the stages of compactness and delatancy, respectively. The acoustic emission occurs during the latter part of the interval CD.

and thus to reduce the intensity of the acoustic emission. In Miwa et al. (1983), it is stated that, 'the squeaky sand produced the sound with relatively high frequency only at the last short period of penetration when the velocity was high and the larger force worked on the sand. The musical sand emitted the audible sound with high sound pressure and relatively low frequency which lasted for a long time'. Point D marks the end of the stage of delatancy and the beginning of the stage of compactness. Point A marks the beginning of the stick stage. The slope of the segment AB, corresponding to a silent sand, was chosen to be 1 in view of the preceding discussion and the lack of any specific information indicating otherwise.

The origin of the hysteresis loop in Fig. 14(b) could lie with the rates of excitation and dissipation of certain elastic modes of vibration in the grains. From Patitsas and Patitsas (1990), Noel and Patitsas (1998), it can be inferred that the circumferential modes of vibration in a thin layer on the surface of the grains are less sensitive to the lack of sphericity of the grains than the thickness modes, where the particle displacement is radial. In the same sense, the torsional modes in the grains are less sensitive to sphericity than the radial modes. It is reasonable to assume that the rate of excitation of these more stable modes depends strongly on the shape and surface texture of the grains and on the degree of confinement of the granular bed. The degree of confinement defines the strength of the shear stress experienced by the grains during the compactness stage, corresponding to the interval AB in Fig. 14(b). Qu et al. (1995) reported that honeycomb-like pits on the surface of quartz grains may play a significant role towards their musical property, while Leach et al. (1995) reported that as the water dries, after milling, the grains become coated with an extremely thin silica layer. In the interval BC and the early part of the interval CD, the energy stored in these modes is converted into fluidization energy. If these modes fail to be excited in the interval AB, the segment BC would fall back on the segment AB, resulting in no hysteresis loop and no sound emission.

From the simple exercise of representing a grain by an elastic circular rod with length equal to its diameter, it follows that when the energy of the fundamental mode is equal to $(1/2)m\bar{v}^2$, the amplitude of oscillation at the end of the rod is equal to 3×10^{-9} m. However, this is only an estimate based on the theory for a thin rod (Kinsler et al., 1993). From Eq. (A.7), with $\rho = 2650\,\mathrm{kg/m^3}$, Young's modulus $E = 7.9 \times 10^{10}\,\mathrm{N/m^2}$, Poisson ratio $\nu = 0.33$, $R = 0.15$ mm and $v_{1\zeta} = \bar{v} = 10$ cm/s, it follows that the maximum surface displacement at the point of contact during collision is $\alpha = 5 \times 10^{-8}$ m. Thus, the energy of the elastic modes in the grains could exceed substantially the grain fluidization energy $(1/2)m\bar{v}^2$.

3.5. Moonquakes and Mars erosion

Criswell et al. (1975) advanced the idea that the thermal moonquakes, which coincide with the beginning of the lunar day, are due to avalanche events on the moon's craters. However, they also argued that the gravitational potential

energy of the granular beds on the surface of the craters is not nearly sufficient to maintain the moonquakes during the estimated geological time of their existence. According to Duennebier and Sutton (1974), the frequency of these emissions is about 5 Hz and their duration is more than 60 s. There is also the appearance of regular interruptions, about every 10 cycles, suggesting stick-slip effects.

Within the context of the acoustic emissions from squeezed granular beds, it is possible that moonquakes originate with granular material being squeezed in the cracks and crevices on the surface of the craters. During the lunar night the temperature drops to an average of -180°C and during the day it rises to an average of 130°C (Kaufmann and Freedman 1999). In the context of this study, the grains tend to fall into the crevices during the night and then are squeezed during the day when the rock masses expand. In this scenario, the solar energy required for the acoustic emissions is nearly limitless.

It was established in the previous section that the frequency of the acoustic emissions from the squeezed grains is of the order of 1000 Hz, which is about 200 times that of the moonquakes. From Eq. (18), it follows that the ratio $V_s/\lambda_d \approx V_s/\beta$ is 200 times smaller on the moon. As in the case of the experiment by Takahara (1973), deep crevices combined with high temperatures and low gravitational acceleration could result in a state of hyper-fluidization, where the phase velocity V_s acquires very low values.

It has been reported recently (National Post on Discovery, 2000) that on the craters of Mars, near and facing the poles where the temperature is at its lowest, there are erosion ridges similar to those formed on earth by flowing water. Beside the possibility of the presence of ice under the surface, which at some time melted and caused the erosion, the possibility of granular avalanches having caused it ought to be considered. Condensation of CO_2 on the grain surface could result in relatively low values of μ and e, resulting in turn in low values of $\bar{v}/\Delta u|_o$. For example, in Fig. 12 the point with $\mu = 0.22$ and $e = 0.30$ lies on the curve with $\bar{v}/\Delta u|_o = 2$, allowing for values of Δu larger than 2 cm/s. The corresponding angle ψ is nearly 13°, which could be considerably smaller than the surface-slope of the craters. As $\bar{v}/\Delta u \to \bar{v}/\Delta u|_o$ in Fig. 11, λ_B becomes sufficiently small to render Eqs. (A.16)–(A.21) inapplicable. From considerations in Section 3.2, it follows that as Δu is increased from about 2–7 cm/s, η could acquire a very low value, giving rise to a water-like fluidized bed. Clearly, the existence of such a state could have important implications in the handling and transport of granular media.

4. Conclusions

Grain flow is a prerequisite to any sonorous acoustic activity of a granular bed. The treatment of a granular bed as a fluidized viscous medium energized by laminar-like flow velocity gradients leads to the prediction of regions of weakness or slip channels. These channels act as the means for grain transport and energy conversion into acoustic modes of vibration, with frequencies defined principally in the surface boundary layer. The width of such channels and the acoustic frequency spectra match the available experimental data fairly well. However, there is no apparent reason why the modes corresponding to two adjacent frequencies are not equally excited. Further, the calculated values of the linear concentration parameter λ_B fall in the expected range of 5–7.

The acoustic phase velocity in the slip channels has the relatively low value of 1 m/s. The dominant frequency of an acoustic emission corresponds to the frequency of the mode of vibration, in a given slip channel, having a wavelength equal to the channel width. The effect of this mode of vibration is the increase-decrease of the distance between layers in the vicinity of the center of the slip channel, which facilitates the slipping of the layers and the transfer of the available mechanical energy into acoustic energy.

The coefficients of friction and restitution and the velocity ratio $\bar{v}/\Delta u$ completely characterize the granular bed. The dependence of $\bar{v}$ on Δu is defined by a hysteresis loop on the $\bar{v} - \Delta u$ plane. For a silent granular bed, the loop degenerates into the straight line $\bar{v} = \Delta u$. The degree of the sonorous property of the granular bed is related to the size of the hysteresis loop. The lack of reproducibility of the frequency spectra can be attributed to their critical dependence on the width and the phase velocity of the boundary layer, and to their dependence on $\bar{v}/\Delta u$, which is history dependent. In analogy with the magnetomotive force H in electromagnetism, Δu can be labeled as 'the fluidomotive force'.

The relatively low value of Δu is consistent with stick–slip, or equivalently, with compactness and delatancy effects, which imply a hysteresis loop. The existence of the stick–slip effects is consistent with the equations of fluid mechanics. It may be argued that the size of the hysteresis loop depends on the degree of excitation of certain elastic modes of vibration in the grains during the compactness stage. The degree of excitation depends on the shape and surface texture of the grains, on the rate of dissipation into heat of the elastic modes, and on the geometry of confinement of the granular bed. Effectively, it depends on the strength of the shear stress experienced by the grains during the compactness stage. The dependence of the degree of singability–boomability of a granular bed on the degree of

excitation of elastic modes in the grains is quite analogous to the dependence of the degree of ringability of a regular bell on the degree of excitation of its elastic modes of vibration. For example, a bell which has been cracked is nearly silent.

For relatively low values of the coefficients of friction μ and restitution e, and for relatively high values of the velocity ratio $\bar{v}/\Delta u$, the granular bed is inherently unsingable or unboomable. However, in most cases the granular bed is silent because the opposite is true, i.e., $\bar{v}/\Delta u$ is too low, resulting in very narrow slip channels placed very close to the surface, resulting in turn in an hyper-energized surface boundary layer. In this case, the granular bed can become singable by altering the geometry of confinement, i.e., by squeezing the grains, resulting in a higher velocity ratio. The rare nature of the booming phenomena can be attributed to the relatively large value of the velocity ratio $\bar{v}/\Delta u$. Effectively, a slight change in the surface texture of the grains can result in a velocity ratio above the limit for boomability. Further, a change in the surface texture can result in reduced excitation of the elastic modes of vibration in the grains during the compactness stage, rendering the granular bed unboomable. The lack of boomability of an avalanching snow bed could be due to the lack of a sufficiently fluidized surface boundary layer.

An increase in $\bar{v}/\Delta u$ in the granular beds trapped in the rock crevices on the surface of the moon's craters could be the cause of the observed thermal moonquakes. These quakes occur during the moon-morning hours when the rock masses undergo expansions due to rapid temperature rise, resulting in the squeezing of the trapped grains. States of hard compactness and of hyper-fluidity are predicted, the latter having obvious implications in the transport and handling of granular materials. The hyper-fluidity state could also have implications on the causes of the erosion ridges recently observed on the craters of Mars.

The conditions under which the equations of fluid mechanics are applicable to moderately fluidized granular beds need to be investigated. The existence of modes of vibration in the sonorous granular beds is supported by the available experimental data. Further investigations of the width of the slip channels and of the boundary layer, and of Δu and λ_B in these regions, will shed more light on the existence and the properties of such modes of vibration.

Acknowledgements

This paper is dedicated to George Freier, who taught the author mechanics at the University of Minnesota, USA, in 1954, and to persevere in seeking to unravel the secrets of nature. Special considerations are due to: Gottfried Rubin, Marcel Leach, Steve Patitsas and Jean Marc Noel for their support towards the completion of this study; to Shigeo Miwa (Japan) for his permission to reproduce parts of his experimental work; to Glenn McDowell for recording the time signals from the frog sand and effecting the fast Fourier transforms; to Jason Hewett, John Theal, Antt Saari and John Viinalass for their assistance with computer and editing questions; to Garry Clark for his contribution towards the completion of the drawings and to Yoko Sasaki (JAPAN) for her assistance in acquiring the frog sand cell.

Appendix A. Collision mechanics in slow granular flows

Fig. 15 depicts sphere A of radius R_1 and mass m_1 colliding with sphere B of radius R_2 and mass m_2 in the laboratory frame specified by axes xyz. The initial and final velocities of sphere A are $\mathbf{v}_1$, $\mathbf{v}_1'$ and those of sphere B are $\mathbf{v}_2$, $\mathbf{v}_2'$ respectively. The axis ζ lies along the surface-normal at the point of contact. The angular velocity of sphere A is $\boldsymbol{\omega}_1 = \omega_1\hat{\eta}$ and that of sphere B is $\boldsymbol{\omega}_2 = \omega_2\hat{\eta}$. From the principle of conservation of linear momentum and the equation

$$(\mathbf{v}_1' - \mathbf{v}_2') \cdot \hat{\zeta} = -e(\mathbf{v}_1 - \mathbf{v}_2) \cdot \hat{\zeta}, \tag{A.1}$$

the following equations are obtained for uninterrupted sliding (Goldsmith, 1960)

$$v_{1\zeta}' - v_{1\zeta} = -\frac{1+e}{1+M}(v_{1\zeta} - v_{2\zeta}), \tag{A.2}$$

$$v_{1\xi}' - v_{1\xi} = -\mu\frac{1+e}{1+M}(v_{1\zeta} - v_{2\zeta}), \tag{A.3}$$

$$v_{2\zeta}' - v_{2\zeta} = \frac{M}{1+M}(1+e)(v_{1\zeta} - v_{2\zeta}), \tag{A.4}$$

$$v_{2\xi}' - v_{2\xi} = \mu\frac{M}{1+M}(1+e)(v_{1\zeta} - v_{2\zeta}), \tag{A.5}$$

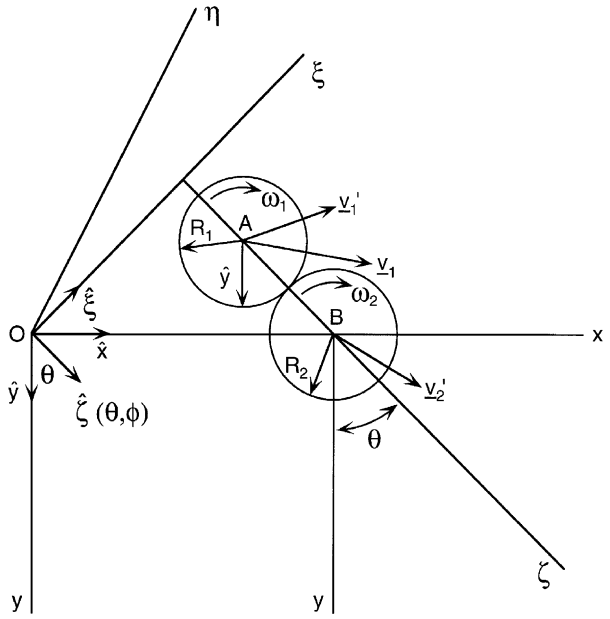

Fig. 15. Schematic of the collision of two spheres, A, B, of radii R_1, R_2, respectively. The velocities after collision are indicated with a prime. The laboratory frame is shown by the axes xyz, with $\hat{z}$ out of the plane of the paper. The ζ axis is along the surface-normal at the point of contact. $\hat{\zeta}$ has polar and azimuthal angles θ, ϕ in the xyz axes. $\hat{\eta} = \hat{\xi} \times \hat{\zeta}$.

where $M = m_1/m_2$, μ is the coefficient of kinetic friction and e is the coefficient of restitution. For interrupted sliding with $M = 1$, the above equations for $v'_{1\zeta}$, $v'_{2\zeta}$ remain the same but

$$v'_{1\xi} = \frac{6}{7} v_{1\xi} + \frac{1}{7} R\omega_1, \qquad v'_{2\xi} = \frac{1}{7} v_{1\xi} - \frac{1}{7} R\omega_1. \tag{A.6}$$

The expression for the maximum normal force f_n at the point of contact during the collision is (Goldsmith, 1960; Timoshenko and Goodier, 1970)

$$f_n = n\alpha^{3/2}, \qquad \alpha = \left[\frac{5\sqrt{2}\pi}{4} \rho \frac{1 - \nu^2}{E}\right]^{2/5} v_{1\zeta}^{4/5} R, \tag{A.7}$$

where α is the maximum surface displacement at the point of contact, $R = R_1 = R_2$, ρ = particle mass density $= (6/\pi)m/d^3$, $n = 2/(3\pi k_1)(R/2)^{1/2}$, $k_1 = (1 - \nu^2)/(\pi E)$, ν is the Poisson ratio and E is the Young modulus of the grains. Further, the time of contact τ_c is written as $\tau_c = 2.94(\alpha/v_{1\zeta})$ (Goldsmith, 1960; Timoshenko and Goodier 1970).

Shen and Ackermann (1982) used Eqs. (A.2)–(A.5) and the assumption that $\omega_1 = \omega_2 = 0$ to derive the following expression for the dissipation energy averaged over the angles θ, ϕ defining the point of impact in Fig. 15.

$$e_c = \frac{1}{2} m(1 + e)\left[\frac{1 - e}{4} + \frac{\mu}{\pi} - \frac{1 + e}{4}\mu^2\right]\bar{v}^2, \tag{A.8}$$

Effectively, e_c is the difference in the kinetic energies before and after a collision and $\bar{v}$ is the fluctuation or the average random grain velocity. It is assumed that due to the relatively close proximity and the generally irregular shape of the grains, the rotational motion has minimal effect. It can be shown that with $v_{2\zeta} = 0$ and $\omega_1 = \omega_2 = 0$ the sliding remains uninterrupted for a time interval Δt, which is related to τ_c as follows:

$$\frac{\Delta t}{\tau_c} = 0.54 \frac{v_{1\xi o} - v_{2\xi o}}{\mu v_{1\zeta}}, \tag{A.9}$$

where $v_{1\xi o}$ and $v_{2\xi o}$ are the velocities of spheres A, B along $\hat{\xi}$ at $t = 0$. With $v_{1\xi o} - v_{2\xi o} = \bar{v}/2$, $v_{1\zeta} = \bar{v}$ and $\mu = 0.5$, $\Delta t/\tau_c = 0.54$. However, this ratio can have larger values when the angular velocities of the grains are not zero and are directed as shown in Fig. 15. In deriving Eq. (A.9), it was assumed that the average force at the point of contact, along $\hat{\xi}$, during collision is equal to $\mu(f_n/2)$. The interruption of the sliding during collision could account for the negative

values assumed by e_c for large values of μ and e. However, for the values of μ and e shown in Table 3 in Section 3.2, e_c has positive values.

On account of the relatively high compactness in the granular bed and the generally small value of $\Delta u/\bar{v}$, the relative velocity before collision is written approximately as

$$\mathbf{v}_1 - v_{2\xi}\hat{\xi} = \bar{v}\hat{y} + \Delta u\hat{x}, \tag{A.10}$$

where on average $v_{2\zeta}$ is assumed to be zero and Δu is the relative velocity between layers in Figs. 1 and 2. In order to obtain expressions for $v_{1\zeta}$ and $v_{1\xi} - v_{2\xi}$, the unit vectors $\hat{\zeta}$, $\hat{\xi}$ are expressed in terms of the unit vectors $\hat{x}$, $\hat{y}$, $\hat{z}$. The unit vector $\hat{\zeta}$ is written in the usual way as, $\hat{\zeta} = \sin\theta\cos\phi\hat{x} + \sin\theta\sin\phi\hat{z} + \cos\theta\,\hat{y}$. However, the expression for $\hat{\xi}$ requires some algebra (Shen and Ackermann, 1982). In general $\hat{\xi}$ is expressed as $\hat{\xi} = a\hat{x} + b\hat{z} + c\hat{y}$, and from the conditions $\hat{\xi}\cdot\hat{\zeta} = 0$, $\hat{\xi}\cdot(\hat{x}\times\hat{\zeta}) = 0$, $|\hat{\xi}| = 1$, it follows that $a = (1 - \sin^2\theta\cos^2\phi)^{1/2}$ and

$$b = a\frac{\sin^2\theta\sin\phi\cos\phi}{\cos^2\theta + \sin^2\theta\sin^2\phi}, \qquad c = a\frac{\sin\theta\cos\theta\cos\phi}{\cos^2\theta + \sin^2\theta\sin^2\phi}. \tag{A.11}$$

Since θ, in general, lies in the range $0 < \theta < \theta_o \approx 40^\circ$, c is considerably smaller than a. Further, $b = 0$ on average when the integration over ϕ is effected, resulting in $\hat{\xi}$ being close to $\hat{x}$. From Eq. (A.10), it follows that

$$v_{1\zeta} = \bar{v}\left(\cos\theta + \sin\theta\cos\phi\frac{\Delta u}{\bar{v}}\right), \qquad v_{1\xi} - v_{2\xi} = \bar{v}\left(c + a\frac{\Delta u}{\bar{v}}\right). \tag{A.12}$$

The momentum transfers to sphere A along $\hat{\zeta}$, $\hat{\xi}$ during the collision are

$$\Delta P_\zeta = -m\frac{1+e}{2}v_{1\zeta}, \qquad \Delta P_\xi = -m\mu\frac{1+e}{2}v_{1\zeta}, \tag{A.13}$$

where Eqs. (A.2) and (A.3) have been used with $v_{2\zeta} = 0$ and $M = 1$. In the laboratory frame xyz, the equations for the momentum transfers along $\hat{x}$, $\hat{y}$ are, $\Delta P_x = a\,\Delta P_\xi + \sin\theta\cos\phi\,\Delta P_\zeta$ and $\Delta P_y = c\,\Delta P_\xi + \cos\theta\,\Delta P_\zeta$.

The point of contact in Fig. 15 lies on the upper back surface of sphere B specified by the angles θ', ϕ', where $\theta' = \pi - \theta$ and $\phi' = \pi + \phi$. For collisions with the contact point on the back part of sphere B, the averages of ΔP_x and ΔP_y are, $\overline{\Delta P}_{xb} = -A_2\bar{v}I_{11} - A_2\,\Delta u I_{12} - A_3\bar{v}I_{13} - A_3\,\Delta u I_{14}$ and $\overline{\Delta P}_{yb} = -A_2\bar{v}I_{21} - A_2\,\Delta u I_{22} - A_3\bar{v}I_{23} - A_3\,\Delta u I_{24}$, where $A_2 = m\mu(1+e)/2$ and $A_3 = m(1+e)/2$. The parameters $I_{1j}, j = 1\ldots4$ are equal to integrations over θ, ϕ, divided by $\pi\theta_o$, of the following functions respectively, $a\cos\theta$, $a\sin\theta\cos\phi$, $\sin\theta\cos\theta\cos\phi$ and $\sin^2\theta\cos^2\phi$. For the parameters I_{2j}, $j = 1\ldots4$, the following functions apply, $c\cos\theta$, $c\sin\theta\cos\phi$, $c\cos^2\theta$ and $\sin\theta\cos\theta\cos\phi$. The limits in the angle ϕ are from $-\pi/2$ to $\pi/2$ and in the angle θ from 0 to θ_o, where θ_o is obtained from Eq. (28). In the context of the present study, the limit angle θ_o assumes values around 40°, while in Shen and Ackermann (1982) it was assumed to be 90°, reflecting a considerably reduced compactness. With $\theta_o = 40^\circ$, the numerical values of I_{ij} are

$$I_{11} = 0.8873, \qquad I_{12} = 0.1970, \qquad I_{13} = 0.1884, \qquad I_{14} = 0.0736,$$

$$I_{21} = 0.1807, \qquad I_{22} = 0.0701, \qquad I_{23} = 0.8526, \qquad I_{24} = 0.1884. \tag{A.14}$$

For collisions with the contact point on the front part of the sphere B, the expressions for the momentum transfers are, $\overline{\Delta P}_{xf} = -A_2\bar{v}I_{11} + A_3\bar{v}I_{13}$ and $\overline{\Delta P}_{yf} = A_2\bar{v}I_{21} - A_3\bar{v}I_{23}$. The terms due to Δu are absent in this case and the terms containing the integrals I_{13}, I_{21} change sign due to the presence of $\cos\phi$.

The normal and the tangential forces per unit area exerted by the layer below on the layer above along $-\hat{y}$ and $-\hat{x}$ are the pressure p and the shear stress σ. With the number of collisions per second between grains A, B assumed to be $1/2(\bar{v}/s)$ and the number of grains per unit area being equal to $1/(d+s)^2$, the expressions for σ and p become

$$\sigma = \overline{\Delta P}_x\frac{1}{(d+s)^2}\frac{1}{2}\frac{\bar{v}}{s}, \qquad p = \overline{\Delta P}_y\frac{1}{(d+s)^2}\frac{1}{2}\frac{\bar{v}}{s}, \tag{A.15}$$

where, $\overline{\Delta P}_x = \overline{\Delta P}_{xb} + \overline{\Delta P}_{xf}$ and $\overline{\Delta P}_y = \overline{\Delta P}_{yb} + \overline{\Delta P}_{yf}$. It follows that

$$\sigma = q_1\rho\frac{d}{s}\bar{v}^2, \tag{A.16a}$$

or

$$\sigma = q_1'\rho\frac{d}{s}\bar{v}\,\Delta u, \tag{A.16b}$$

and

$$p = q_2 \rho \frac{d}{s} \bar{v}^2, \tag{A.16c}$$

where

$$q_1 = \frac{1+e}{4}\left[2\mu I_{11} + (\mu I_{12} + I_{14})\frac{\Delta u}{\bar{v}}\right], \tag{A.17a}$$

$$q_1' = q_1 \frac{\bar{v}}{\Delta u}, \tag{A.17b}$$

$$q_2 = \frac{1+e}{4}\left[2I_{23} + (\mu I_{22} + I_{24})\frac{\Delta u}{\bar{v}}\right]. \tag{A.18}$$

Eq. (A.16c) is referred to as the equation of state in Haff (1983). The dynamic angle of sliding ψ is defined as

$$\tan\psi = \frac{\sigma}{p} = \frac{q_1}{q_2}. \tag{A.19}$$

For $\bar{v}/\Delta u \gg 5$, about, it reduces to $\tan\psi \approx \mu(I_{11}/I_{23})$. In general, ψ depends weakly on $\Delta u/\bar{v}$ since the dominant integrals are I_{11} and I_{23}. The viscosity coefficient η is defined by the equation

$$\sigma = -\eta \frac{\mathrm{d}u}{\mathrm{d}y}. \tag{A.20}$$

From Eq. (A.16) and with $\mathrm{d}u = \Delta u$, $\mathrm{d}y = d$, the expression for η becomes

$$\eta = q_1' \rho d^2 \frac{\bar{v}}{s} \quad \text{or} \quad \eta = \frac{q_1'}{q_2}\frac{pd}{\bar{v}}. \tag{A.21}$$

From Eq. (A.17b), η can be written similarly with $q_1/\Delta u$ in place of $q_1'/\bar{v}$. In the context of the kinetic theory of gases, η is proportional to Δu according to Thompson (1993). From Eq. (A.21), with $q_1 = 0.5$, $\bar{v}/\Delta u = 5$, $\bar{v} = 10\,\mathrm{cm/s}$, $\rho = 1700\,\mathrm{kg/m^3}$, $d = 0.5\,\mathrm{mm}$, $\lambda_B = 10$, $\eta = 2\,\mathrm{kg/(ms)}$, while η for water at 20°C is $10^{-3}\,\mathrm{kg/(ms)}$.

In the context of the theory of fluid mechanics (Haff, 1983; Ryhming, 1985; Lu, 1973), the equation of motion of a fluidized grain bed becomes the Navier–Stokes equation, i.e.,

$$\frac{\partial}{\partial t}(\rho u_i) = -\frac{\partial p}{\partial x_k}\delta_{ik} - \rho u_k \frac{\partial u_i}{\partial x_k} + \frac{\partial}{\partial x_k}\left(\eta\frac{\partial u_i}{\partial x_k} + \eta\frac{\partial u_k}{\partial x_i}\right) + \rho g_i, \tag{A.22}$$

where ρ is the mass density, u_i are the particle velocity components and g_i are the gravitational acceleration components. Effectively, the left-hand side is the mass per unit volume times the acceleration, while the right-hand side is the sum of all forces acting on the unit volume. The indices $i = 1, 2, 3$ and $k = 1, 2, 3$ correspond to the axes xyz in Fig. 2 and the repeated index k implies summation over k. With $i = x$, $u_y = u_z = 0$ and no variation with respect to x, z, Eq. (A.22) reduces to

$$\rho\frac{\partial u_x}{\partial t} = \frac{\partial}{\partial y}\left(\eta\frac{\partial u_x}{\partial y}\right) + \rho g_x. \tag{A.23}$$

A similar equation can be written for p, with $i = y$. For steady state motion $\partial u_x/\partial t = 0$, $\partial u_y/\partial t = 0$, resulting in

$$\sigma = \rho g_x y + C_1, \tag{A.24a}$$

$$p = \rho g_y y + C_2. \tag{A.24b}$$

In the case of the avalanching sand, C_1 and C_2 are 0. The energy equation for a fluidized granular bed is (Haff, 1983; Ryhming, 1985)

$$\frac{\partial}{\partial t}\left(\frac{1}{2}\rho u^2 + \frac{1}{2}\rho\bar{v}^2\right) = -\frac{\partial}{\partial x_k}\left[\rho u_k\left(\frac{p}{\rho} + \frac{1}{2}u^2 + \frac{1}{2}\bar{v}^2\right) - \eta u_i\frac{\partial u_i}{\partial x_k} - K\frac{\partial}{\partial x_k}\left(\frac{1}{2}\rho\bar{v}^2\right)\right] + \rho u_i g_i - I, \tag{A.25}$$

where I is the energy sink, i.e., the energy converted into heat per unit volume per second due to the inelastic nature of the grain collisions and K is the thermal diffusivity coefficient. In the steady state without variation with x, z and with

$k = y$, $u_z = 0$, Eq. (A.25) reduces to

$$\frac{\partial}{\partial y}\left[\eta u_x \frac{\partial u_x}{\partial y} + K\frac{\partial}{\partial y}\left(\frac{1}{2}\rho\bar{v}^2\right)\right] + \rho u_x g_x + \rho u_y g_y - \frac{\partial}{\partial y}(p u_y) - I = 0. \tag{A.26}$$

In deriving Eq. (A.26), the terms $(1/2)u^2$, $(1/2)\bar{v}^2$ were omitted in comparison with $p/\rho = gh \approx 1$ for the avalanching sand. The error in omitting these terms is even smaller for the forced sand. It is shown in Section 2.2.2 that $u_y \ll u_x$, implying that the term $\eta u_y(\partial u_y/\partial y)$ can be neglected in comparison with the term $\eta u_x(\partial u_x/\partial y)$.

The term $\partial/\partial y[K\partial/\partial y((1/2)\rho\bar{v}^2)]$ is viewed as the divergence along $\hat{y}$ of the fluidization energy flux density Q, defined as

$$Q = K\frac{\partial}{\partial y}\left(\frac{1}{2}\rho\bar{v}^2\right). \tag{A.27}$$

Haff (1983) argued that the mean fluidization energy transfer per unit area per second along $\hat{y}$ can be written as

$$Q = \frac{m\bar{v}\,\Delta\bar{v}}{d^2}\frac{\bar{v}}{2s} = d^2\frac{\bar{v}}{2s}\frac{\mathrm{d}}{\mathrm{d}y}\left(\frac{1}{2}\rho\bar{v}^2\right), \tag{A.28}$$

where $\Delta\bar{v}$ is the fluctuation velocity difference between adjacent layers. Comparison with Eq. (A.27) reveals that

$$K = d^2\frac{\bar{v}}{2s}. \tag{A.29}$$

Upon using Eqs. (A.20) and (A.24), Eq. (A.26) reduces to

$$\frac{\sigma^2}{\eta} + K\frac{\partial^2}{\partial y^2}\left(\frac{1}{2}\rho\bar{v}^2\right) + \frac{\partial K}{\partial y}\frac{\partial}{\partial y}\left(\frac{1}{2}\rho\bar{v}^2\right) - p\frac{\partial u_y}{\partial y} - I = 0. \tag{A.30}$$

From Eq. (A.24b), it follows that the terms $-\partial p/\partial y$ and $\rho g_y u_y$ cancel out in Eq. (A.26). The term σ^2/η represents the mechanical energy input into the granular bed per unit volume per second by the shear forces driving it. This can be seen by expressing this energy input as, $\sigma\Delta u/d = \sigma\partial u_y/\partial y = \sigma^2/\eta$, from Eqs. (A.20) and (A.24). Similarly, the term $-p\partial u_y/\partial y = -p\,\Delta u_y/d$ represents the mechanical energy flowing out of the granular bed per unit volume per second during delatancy, where the velocity Δu_y is the difference in u_y between adjacent layers. The dissipation energy I is written as $I = e_c(r_c/d^3)$, where e_c is given by Eq. (A.8) and r_c, the collision rate, is given as $r_c = 1/2(\bar{v}/s)$. Consequently, the expression for I becomes

$$I = \Gamma\rho\frac{\bar{v}^3}{s}, \quad \Gamma = \frac{1+e}{4}\left[\frac{1-e}{4} + \frac{\mu}{\pi} - \frac{1+e}{4}\mu^2\right]. \tag{A.31}$$

References

Abramowitz, M., Stegun, I.A., 1964. Handbook of Mathematical Functions. Dover Publications Inc., New York, pp. 355–374.

Bagnold, R.A., 1941. The Physics of Blown Sand and Desert Dunes. Chapman & Hall, London, pp. 247–257.

Bagnold, R.A., 1954. Experiemets on a gravity-free dispersion of large solid spheres in a newtonian fluid under shear. Proc. Roy. Soc. 225A, 49–63.

Bagnold, R.A., 1966. The shearing and dilataion of dry sand and the singing mechanism. Proc. Roy. Soc. 295A, 219–232.

Barber, P.W., Yeh, C., 1975. Scattering of electromagnetic waves by arbitrarily shaped dielectric bodies. Appl. Opt. 14, 2864–2872.

Bolton, H.C., 1889. Researches on sonorous sand in the Peninsular of Sinai. Proceedings of the American Association for the Advancement of Science 38, 137–159.

Brown, A.E., Campbell, W.A., Robson, D.A., Thomas, E.R., 1961. Musical sand: the singing sands of the seashore part I. Proc. Univ. Durham Philos. Soc. 13 (21), 217–230.

Brown, A.E., Campbell, W.A., Jones, J.M., Thomas, E.R., 1964. Musical sand: the signing sands of the seashore part II. Proc. Univ. Newcastle Upon Tyne Philosophical Society 1, 1–21.

Cowin, S.C., 1978. Milrostructural continuum models for granular materials. In: Cowin, S.E., Satake, M. (Eds.), Proceedings of the US–Japan Seminar on Continuum-Mechanical and Statistical Approaches in the Mechanis of Granular Materials. Gakujutsu Bunken Fukyukai, Tokyo, Japan, pp. 162–170.

Criswell, D.R., Lindsay, J.F., Reasoner, D.L., 1975. Seismic and acoustic emission of a booming dune. Journal of Geophysical Research 80, 4963–4974.

Duennebier, F., Sutton, G.H., 1974. Thermal moonquakes. Journal of Geophysical Research 79, 4351–4363.

Goldsmith, W. 1960. Impact: The Theory and Physical Behaviour of Colliding Bodies. Edward Arnold Ltd., London, pp. 83–91.

Goldsmith, W., 1952. The Coefficient of Restitution. American Society for Engineeging Education, Mechanics Division, Mechanics Division Bulletin, May 1952, pp. 1–4.

Haff, P.K., 1983. Grain flow as a fluid mechanical phenomenon. Journal of Fluid Mechanics 134, 401–430.
Haff, P.K., 1986. Booming dunes. American Scientist 74, 376–381.
Humphries, D.W., 1966. The booming sand of Korizo, Sahara, and the squeaking sand of Gower, S. Wales: a comparison of the fundamental characteristics of two musical sands. Sedimentology 6, 135–152.
Jaeger, H.M., Nagel, S.R., 1992. Physics of the granular state. Science 255, 1523–1530.
Kaufmann, W.J., Freedman, R.A., 1999. Universe, 5th Edition New York, W. H. Freeman and Co., pp. 219–242.
Kilkenny, C., Leach, M.F., Goldsack, D.E., 1997. The acoustic emission of silica gel. Canadian Acoustics 25, 28.
Kinsler, L.E., Frey, A.R., Coppens, A.B., Sanders, J.V., 1982. Fundamentals of Acoustics 3rd Edition, John Wiley & Sons New York, pp. 102–141.
Lapalme, R., Patitsas, A.J., 1993. Light scattering by anthophylite–crocidolite asbestos fibers. Part I. The domain of covergence of the EBCM theory. Particle and Particle System Characterization 10, 111–117.
Leach, M.F., Rubin, A.G., 1990. The acoustics of booming sand. Progress in Acoustic Emissioon V, Proceedings of the 10th International Acoustic Emission Symposium Sendai Japan, The Japanese Society for Non-destructive Inspection, Japan, pp. 239–244.
Leach, M.F., Chartrand, H.J., 1994. Recent progress in the developement of musical sand. Progress in Acoustic Emission VII. The Japanese Society for Non-destructive Inspection, Japan, pp. 499–504.
Leach, M.F., Goldsark, D.E., Chartrand, H.J., 1995. Grain composition and surface characteristics of musical sand. Proceedings of the IEEE Ultrasonics Symposium, Seattle, Washington, pp. 657–659.
Lewis, A.D., 1936. Roaring sands of the Kalahari Desert. South African Geographical Journal 19, 33–50.
Lindsay, J.F., Criswell, D.R., Criswell, T.L, Criswell, B.S., 1976. Sound producing dune and beach sands. Geological Society of America Bulletin 87, 463–473.
Lu, P.-C., 1973. Introduction to Mechanics of Viscous Fluids. New York, Holt, Rinehart & Winston, pp. 400–402.
Miwa, S., Hidaka, J., Shimosaka, A., 1983. Musical sand. Powder Science and Technology in Japan, KONA 1, 64–72.
National Post on Discovery. National Post, June 23, 2000. Toronto, Ontario, Canada, p. A15.
Nishiyama, K., Mori, S., 1982. Frequency of sound from singing sand. Japanese Journal of Applied physics 21, 591–595.
Noel, J.A., Patitsas, A.J., 1998. Modes of vibration in an ideal fluid bounded by two eccentric rigid infinite circular cylindrical boundries. Canadian Journal of Physics 76, 729–738.
Nori, F., Sholtz, P., Bretz, M., 1997. Booming sand. Scientific American 277, 84–89.
Ogawa, S., 1978. Multitemperature theory of granular materials. In: Cowin, S.E., Satake, M. (Eds.), Proceedings of the US–Japan Seminar on Continuum-Mechanical and Statistical Approaches in the Mechanics of Granular Materials. Gakujutsu Bunken Fukyukai, Tokoyo, Japan, pp. 208–217.
Patitsas, S.N., Patitsas, A.J., 1990. Vibrations in a fluid layer between an elastic or rigid sphere and a concentric elastic or rigid shell. Journal of Fluids and Structures 4, 203–217.
Poynting, J.H., Thomson, J.J., 1922. Textbook of Physics; Sound. London, Charles Griffin, pp. 134–145.
Qu, J., Sun, B., Zhang, W., Wang, Y., Kang, G., 1995. Surface texture of quartz grain in booming sand and its acoutic significance. Chinese Science Bulletin 40, 1719–1723.
Ridgway, K., Scotton, J.B., 1973. Whistling sand beaches in the British Isles. Sedimentolgy 20, 263–279.
Ryhming, I.L., 1985. Dynamique des Fluides. Presses Polytechniques Romandes, Paris, pp. 196–198.
Savage, S.B., 1978. Experiments on shear flows of cohesionless granular materials. In: Cowin, S.E., Satake, M. (Eds.), Proceedings of the US–Japan Seminar on Continuum-Mechanical and Statistical Approaches in the Mechanics of Granular Materials. Gakujutsu Bunken Fukyukai, Tokyo, Japan, pp. 241–257.
Shand, E.B., 1958. Glass Engineering Handbook. New York, McGraw-Hill Book Company, Inc., pp. 45–46.
Shen, H., Ackermann, N.L., 1982. Constitutive relations for fluid–solid mixtures. Jounal of the Engineering Mechanics Division 108, 748–763.
Sholtz, P., Bretz, M., Nori, F., 1997. Sound-producing sand avalanches. Contemporary Physics 38, 329–342.
Takahara, H., 1973. Sounding mechanism of singing sand. Journal of the Acoustical Society of America 53, 634–639.
Thompson, P.A., Grest, G.S., 1992. Granular flow at low shear rates. In: Mareschal, M., Holian, B.L. (Eds.), Microscopic Simulutions of Complex Hydrodynamics. Plenum Press, New York, pp. 403–412.
Thompson, P.A., 1993. Vibrated granular assemblies: fluidization and convection. In: Landau, D.P., Mon, K.K., Schuttler, H.B. (Eds.), Computer Simulations in Condensed Matter Physics VI. Spinger Verlag, Berlin, pp. 1–17.
Timoshenko, S.P, Goodier, J.N., 1970. Theory of Elasticity, 3rd Edition. McGraw-Hill Book Co., New York, pp. 409–421.
Winterkorn, H.F, Fang, H-Y., 1975. Foundation Engineering Handbook. NewYork, van Nostrand Reinhold company, pp. 689–690.